POLITECNICO
MILANO 1863

SCUOLA DI INGEGNERIA INDUSTRIALE
E DELL'INFORMAZIONE

DESIGN AND DEVELOPMENT OF A COMPLIANT ELBOW EFFORT-COMPENSATION DEVICE

DOCTORAL PROGRAMME IN BIOENGINEERING

Author: **Emir Mobedi**

Student ID: 10762484
Advisor: Dr. Ajoudani Arash, Prof. De Momi Elena
Tutor: Prof.Raffaele Dellaca'
Academic Year: 2022-23

Abstract

The use of assistive technologies in industrial environments to improve human ergonomics and comfort in repetitive and high effort tasks has increased considerably in the last decade. Predominantly, the goal is to provide additional physical support through lightweight and wearable devices, without posing major constraints to the human body movements. Towards achieving this objective, this thesis introduces design and control of an assistive device for the elbow joint. The contribution of the thesis is classified into two steps. Part I contributions cover the design and its overall validation through classical control techniques. To begin with, the proposed assistive device is easily wearable, lightweight, and cable-driven using a series elastic actuation principle implemented by an endless shape elastic bungee element. This type of elastic element is selected due to its intrinsic damping, and compliant features similar to human muscles, which provides mechanical filtering against dynamic uncertainties such as impulsive forces, and oscillated movements because of possible controller issues.

Furthermore, a spool system is designed targeting to maximize the transmission of the generated elastic force to the wearer while avoiding multiple coiling for the cable wrap/release operation. The design parameters of the device are selected through design and optimization studies. The manufactured actuator's performance is validated on a rigid link under position and force control modes. To demonstrate the effectiveness of the elastic element, actuator validation tests were conducted with and without bungee. The results show that while the bungee-integrated setup can transfer the generated elastic force to the link without oscillation at different frequency movements ($0.05 - 0.16$ Hz), the bungee-excluded setup yields unstable movements under the same control gains, producing 50.74% more vibrations detected through FFT analysis. In addition, to test the system under aggressive conditions, impacts were applied to it, and the results indicate that the damping ratio index of the bungee incorporated system is 56.14% more than that of without bungee case, demonstrating the intrinsic safe behavior of the mechanism. Finally, the device is assessed on 6 human subjects (different arm weights and dimensions) in a simulated industrial painting task with 5 minutes duration, with an average $22.3°/s$ elbow velocity under force control. The average effort reduction on biceps muscle among the subjects is

measured 64.42% with respect to the without assistance test.

Part II contributions are presented to operate the device in more complex tasks. To clarify, the focus of part II studies is to design a reactive control strategy for loading and sudden unloading of an elbow effort-compensation device controlled in force. Through this control strategy, in addition to an individual's forearm weight, an external load can be detected and adaptively compensated via a feed-forward force reference, facilitating the execution of arbitrary movements by the wearer. In case of a sudden contact/load loss, a power-aware strategy is implemented to immediately eliminate the portion of external loading in the force reference. The adaptive compensation of the external loads is achieved through an electromyography interface. Instead, to react to sudden load releases, a power limit is set on the tendon, and continuously measured through an encoder and a load cell connected with the cable. Two sets of experiments are designed to test the proposed load-releasing method on a bench-top setup with 2 kg, and 3.9 kg, and a human subject with 0.5 and 1 kg. Next, the overall scenario including load-compensation and load-releasing are carried out on eight human subjects with 0.5 and 1 kg loads to evaluate the release and compensation time, and the effort reduction with respect to non-powered exoskeleton case. Results show that the average compensation/release time (payload) among subjects is measured as 0.98/0.91 seconds (0.5 kg), and 1/0.86 seconds (1 kg). The average effort reduction among the subjects are also reported as 66.4%, and 67.11% for 0.5 kg, and 1 kg, respectively.

Keywords: Wearable assistive device, exoskeleton design, effort-compensation device, elbow support device, series elastic actuation (SEA), control of assistive devices, power-aware load-releasing control, EMG-based control.

Contents

1 | Introduction

1.1. Motivation

Exoskeleton is derived from a Greek term (Exo-skeleton) referring to the external skeleton of an animal or vegetal [63, 66]. Over the past two decades, exoskeletons have had a prominent role to augment human power by applying assistive forces parallel to the body segments. In contrast to collaborative robots where the human operator only interacts with the robots' end-effector to achieve some collaborative tasks such as aiding humans in an assembly operation [61], these wearable devices can transfer a wide range of assistive torques for different human limbs interacting with them at multiple points. The aforementioned assistive torques vary depending on the targeted application.

Mainly, activities of daily living (ADL), and medical treatment tasks are achieved with the help of these assistive devices. The former covers military [3, 64, 71], industrial [33, 48, 55], and medical [20, 36, 44] applications where the wearers do not have any physical impairments (see Fig.1.1), and the goal is to reduce the effort at the supported joints in repetitive tasks such as reducing the fatigue of a caregiver in a stroke therapy [45], and tool handling [47]. Instead, the latter corresponds to robot-aided physical rehabilitation [62, 67], in which the assistive device is controlled considering the physician's command to recover the injured human limb of the patient.

Moreover, exoskeletons are divided into two categories to be rigid [13, 15, 29] and soft [5, 27, 64]. Rigid wearable devices are built using metal frame in the body attachment which acts as a transmission element between power source, where the assistive force is generated, and the targeted human limb. They are also classified as active [28, 69] and passive [39, 46] among each other. Rigid-passive devices does not contain any electromechanical elements (i.e., motors and sensors), and provide assistance through the elongation of elastic elements for lower-limbs [59], and upper-limbs [63]. Particularly for the shoulder support devices, although they are lightweight, and have a compact size, the mechanism constantly generates assistive force in an upward direction to counterbalance the shoulder, which causes discomfort during repetitive flexion-and-extension movements. Hence, the

exoskeleton itself can lead to creating a disorder in the shoulder [21, 22, 51].

When it comes to rigid-active devices, they are equipped with motors and sensors, allowing to employ extensive flexibility, and better control. However, the fundamental challenge of such devices is the misalignment between the assisted human joint and the exoskeleton axis [10]. To clarify, the kinematics of human joint is complex, and it cannot be modeled simply collecting the kinematic pairs. Moreover, it is not possible to detect the actual configuration of the human limb without making use of particular imaging equipment. Also, the position of the human limb varies with respect to exoskeleton every therapy session [11, 53, 54]. Therefore, the design of rigid-active exoskeletons are quite complex to mechanically mimic the human limbs' kinematic, and they are usually grounded due to their bulky structure.

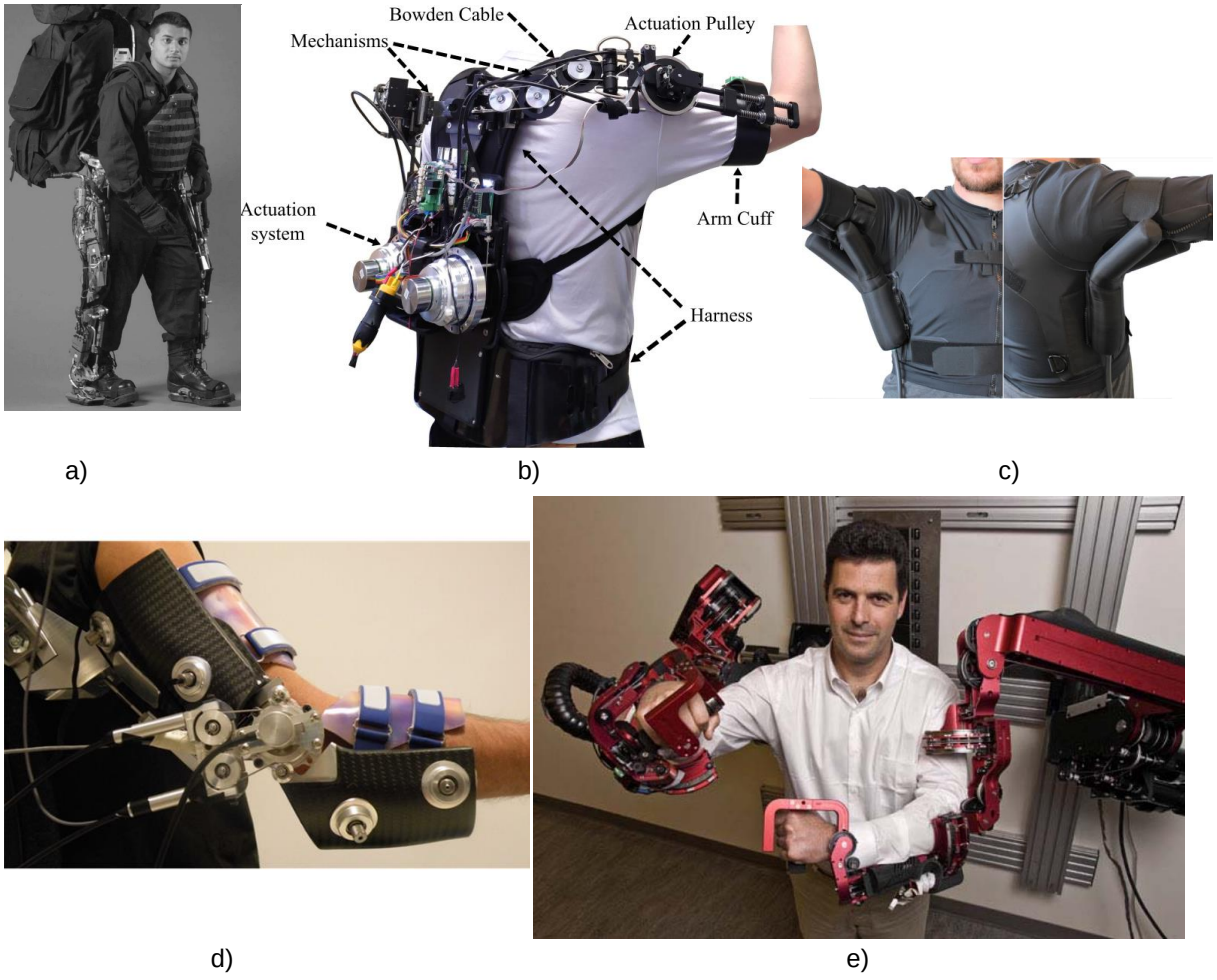

Figure 1.1: (a) Exoskeletons for military [71], (b) industry [47], (c) medical [44], (d) elbow rehabilitation [62], and (e) upper-arm rehabilitation [67] applications.

To overcome the problem of misalignment, soft-active wearable devices are developed utilizing soft body attachments, performing intrinsic adaptation to the targeted human limb. Primarily, the actuation part of those exoskeletons is attached distally from the user such as at the back, and the generated assistive force is transmitted to the human limb with the help of a tendon. This design approach prevents the user to carry the actuation mechanism on the supported joints, which improves the comfort of the wearer. Although their assistive torque range is lower than that of rigid-active devices, they are portable and lightweight, which increases their flexibility and task performance in ADL tasks such as in industry [41] and walking [69].

1.2. Related Works in ADL Exoskeletons

Recent advances in industry pave the way for the need for soft-active assistive devices. To begin with, automated manufacturing is an essential model of the fourth industrial revolution (Industry 4.0) [60]. The primary aim of this breakthrough is to apply decentralized intelligence towards possible problems in the manufacturing lines. Despite the demand to fully or partially automate risky and difficult-for-human industrial tasks (especially for those that require high-payload [19]), transferring the human movement capabilities, flexibility, and decision-making to cobots, and the cooperation of the actions in the most productive, yet intrinsically safe manner, are still a problem for such automation scenarios [24].

Specifically, manual operations such as packaging [43] and assembly [60] still account for a large proportion of tasks in this area. For instance, more than 10.8 million workers are employed in the European Union to handle for storage and transportation of several products in warehouses [18]. As a consequence, according to a recent industry report, such repetitive industrial applications have contributed to a growth in work-related-musculoskeletal disorders (WMSDs) engaging 20% of the global population [18, 51].

To boost the productivity, ergonomics, and physical performances of the human workers in ADL (i.e., manual operations), soft-active wearable assistive devices have shown a great potential for sit-to-stand [69], material handling [47], and walking [34],[68] in the last decade. Considering the actuation unit of such devices, there are several approaches such as electric motor-tendon, shape memory alloy, pneumatic artificial muscles (PAM), pneumatic interference actuators (PIA), and twisted string actuators (TSA) [66].

1.2.1. Design of ADL Exoskeletons

Here, the designs of upper-limb soft-active exoskeletons are discussed to reveal their advantages and disadvantages. In [56], an elbow exosuit is developed to be used for repetitive lifting tasks in manufacturing lines making use of an array of small inflatable cylindrical actuators (i.e., pneumatic interference actuator) and placed on the arm. When it is pressurized, the actuators react to each other and support the user for bending motion at the elbow joint. The primary drawback of the system is to locate the air tank in dynamic environments such as in factories (see Fig.1.3b).

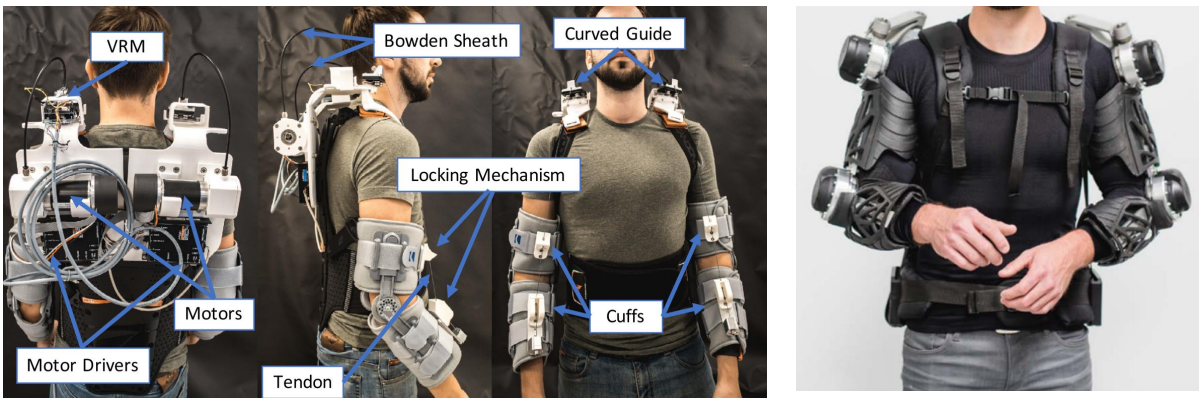

Figure 1.2: (a) A voice activated bi-articular exosuit for upper limb assistance [31], (b) an exoskeleton for industrial applications [16].

More recently, a soft shoulder exoskeleton is designed utilizing a hyper-redundant kinematic chain whose fundamental advantage is to be intrinsically compliant, and kinematically adaptable to the shoulder motion pattern [57]. However, the device can generate up to ≈ 5 Nm assistive torque with 2.45 kg actuation system attached on the shoulder. Not only the exoskeleton is heavy due to its gear transmission system, but also such a design approach increases the reflected inertia on the wearer, reducing the flexibility, and comfort in ADL tasks (see Fig.1.3c). In the same fashion, a wearable device is built to support both the shoulder and elbow of the user in industrial tasks [16]. As the actuation units of the exoskeleton are placed on the human limb, the inertia of the mechanism increases the user's effort during the assistance (see Fig.1.2b).

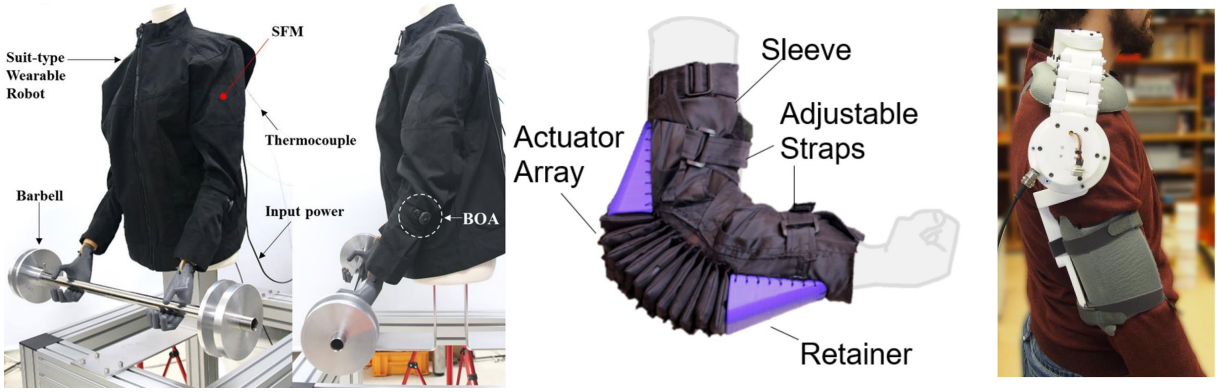

Figure 1.3: (a) Shape-memory-alloy-based-fabric-muscle (SFM) assistive device [49], (b) an elbow exoskeleton based on array of small inflatable cylindrical actuator [56], (c) a soft shoulder exoskeleton based on a hyper-redundant kinematic chain for ADL applications [57].

In another work [30], an upper-limb assistive device is designed to aid workers in industrial tasks. A voice control strategy is employed to generate position trajectory at the shoulder and elbow joints of the dual arm. The device can help the user lift up to 10 kg with the help of 4 motors with a gear system. The total weight of the exoskeleton (excluding the battery) is 10 kg, which is quite heavy, leading to testing the device at a slow-moving task. In [31], a similar control strategy is used to support the shoulder and elbow limbs making use of the under-actuation principle, which allows controlling the two limbs through a single motor. In addition, a locking mechanism is integrated to operate the device in such a way that when the elbow reaches 90°, this mechanism is disengaged to initiate the shoulder movement. Although the under-actuation technique seems an appealing solution to reduce the motor quantity of the exoskeleton (7.5 kg weight, 10 kg payload at hand), it is not possible to control independently the aforementioned two limbs (see Fig.1.2a). Moreover, voice control is not safe for industrial applications as the noise of machines and the environment can mislead the controller.

Furthermore, shape-memory-alloy-based-fabric-muscle (SFM) assistive device is designed for elbow joint to be used for ADL applications [49]. When the shape-memory-alloys are exposed to external Joule heating, the shape of the material changes and create support at the limb. Even though the actuation system of the device weighs less than 1 kg, these actuators suffer from low efficiency, and bandwidth [66]. Moreover, the developed device is not tested on a human (see Fig.1.3a).

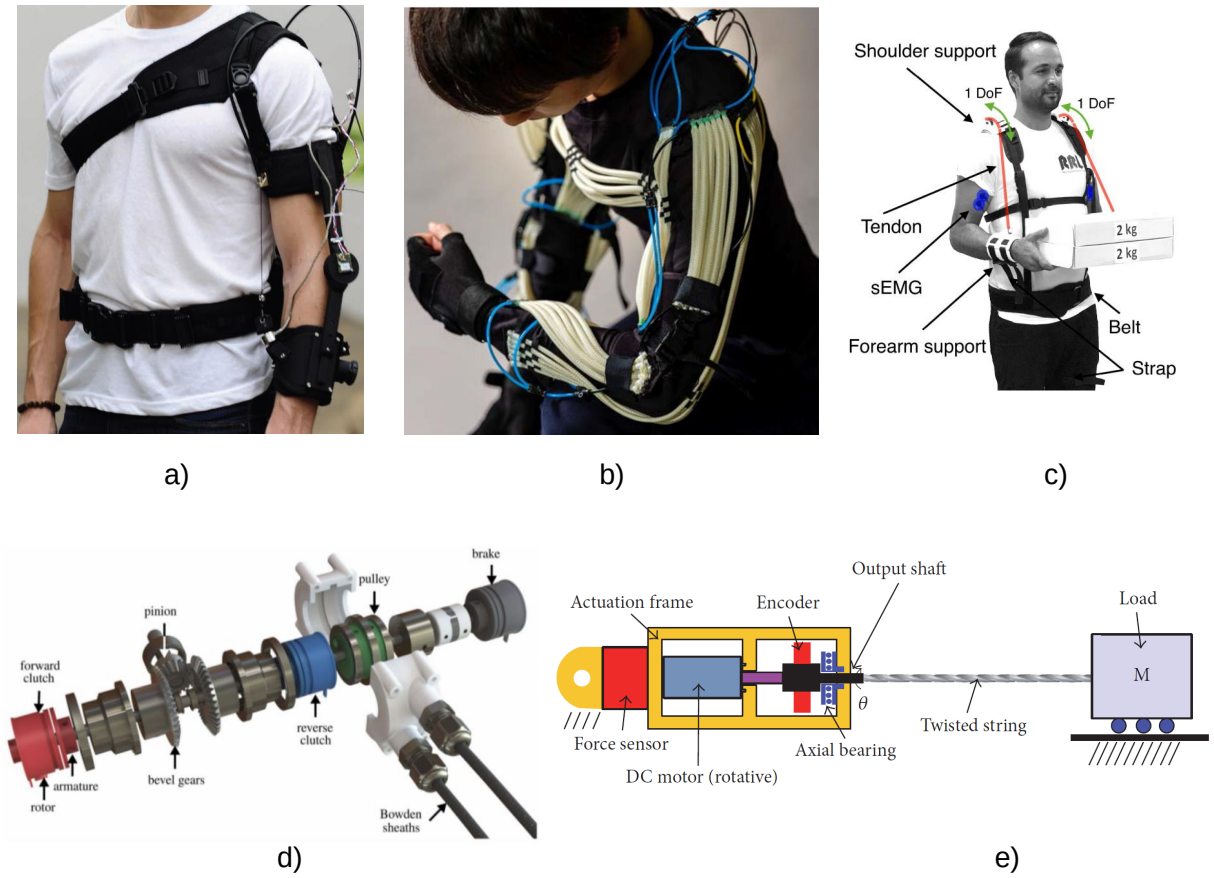

Figure 1.4: (a,d) An elbow exoskeleton based on electric motor-tendon unit [65], (b) pneumatic artificial muscles [1], and (c,e) twisted string actuators [23].

Also, PAMs can be a good approach to developing a lightweight exoskeleton for repetitive ADL tasks. In [1], an active flexible weave structure is designed by making use of the McKibben muscle (see Fig.1.4b). Such muscle includes a rubber tube sheltered by a sleeve. When the air is pressurized inside the rubber tube, it enlarges in the radial direction. This deformation of the sleeve applies a force and displacement in the axial direction of contraction. Furthermore, the flexible weave structure is placed to connect the upper arm to the back (thigh element of the brace), and to assist in lifting the arm in an upward direction. Even though the weight of the exoskeleton is 2.1 kg, it is not possible to use the device in dynamic operations. Also, the maximum torque at the shoulder joint is acquired to be $\approx$ 4 Nm, preventing to carry heavier loads using this device. Since the source of the actuator is air, increasing the payload requires a larger air tank or a compressor which limits the flexibility of the exoskeleton.

Additionally, TSAs have an important role in the area of soft-active exoskeletons as they have a good output force to actuator weight ratio. According to the working principle,

a DC motor is coupled to a few strings whose endpoint is connected to the load (see Fig.1.4e). When the motor is rotated, the total length of the string is decreased to apply linear force to the load. Hence, the rotational motion of the motor is transformed into a linear motion. An elbow exoskeleton is developed utilizing such TSA system in [23]. Although the device is lightweight compared to the existing assistive devices, the load compensation is tested at a single 90° position (see Fig.1.4c).

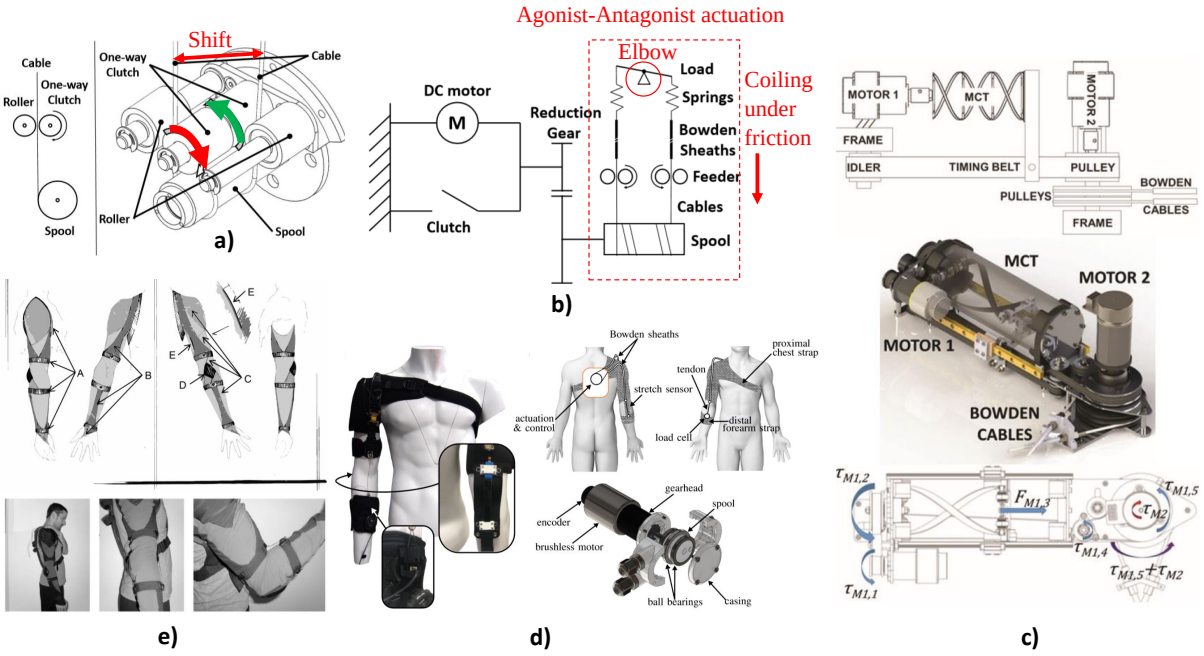

Figure 1.5: (e) The body attachment, and (a,b) agonist-antagonist type actuation system of an elbow exoskeleton [8], (d) an elbow exoskeleton with direct-drive based actuation system [12], (c) multi-stable composite transmission (MCT) system based actuation mechanism for an elbow assistive device [9] .

Furthermore, an electric motor-tendon unit type actuation system is used in an elbow exoskeleton (see Fig.1.4a). One-to-many (OTM) design approach is employed [65], which allows controlling more degrees of freedom than that of the applied input (i.e., under-actuation strategy). In the actuator, there is a DC motor coupled with a pinion gear to transmit the input torque to the bevel gears, allowing to transmit the input torque 90°. Moreover, two clutch mechanisms are used to allow engage/disengage the input torque with the countershaft and a pulley (see Fig.1.4d). Regarding the working principle, if the input pinion is not rotated by the motor, the wearer is free to move, and the output is back-drivable (no assistance). In other words, the flexion/extension movement can be performed since the countershaft is not engaged with neither left nor right bevel gears. In another state, the brake locks the countershaft, and movement is stopped. For the support

in CW (clockwise), and CCW (counterclockwise) directions, the left bevel gear and right bevel gears are coupled with the corresponding clutches, respectively. However, there is no elastic element between actuators and the human limb to achieve a smooth change between states and compensate for unexpected controller issues. Also, the mechanical design is complex, and this affects the movement smoothness during the assistance.

In another design, an agonist-antagonist type actuation system is integrated into an elbow exoskeleton to be used for industrial tasks [8]. The stiffness around the elbow is varied by the DC motor, the gear system, and the springs illustrated in Fig.1.5b. A clutch system is also integrated to stop the release of the cable after setting the stiffness in Fig.1.5a. However, such a solution consumes constantly energy (0.25 A, 24 V). On the other hand, the advantage of the mechanism is to incorporate an elastic element between DC motor and the elbow to absorb the unexpected impacts that may happen during the assistance. However, a feeder assembly is coupled to prevent cable slack during the coiling operation of the spool. For the uncoiling, a one-way clutch is utilized to allow the cable to pass under friction. Hence, in addition to the friction of tendon-driven based force transmissions, adding extra feeder assembly amplifies such nonlinear effects causing a power loss, and also prevents to conduct smooth dynamic movements.

In the next design, multi-stable composite transmission (MCT) system, which is composed of multilayered carbon fiber/epoxy laminates, is used to generate stiffness for elbow support [6]. The system is operated in such a way that the twist of MCT leads to vary the stiffness of the timing belt connected to the output shaft (see Fig.1.5c). The increase of the output torque requires to increase the length of the MCT by twisting. Instead, the stiffness reduction is achieved by rotating it in the opposite direction. The main disadvantage of the mechanism is to generate highly non-linear output stiffness, which gives rise to some control problems [9]. Moreover, the maximum output torque of the device is 6 Nm while the weight is 2.2 kg, which is heavy with respect to the other existing soft-active exoskeletons.

1.2.2. Control of ADL Exoskeletons

In this chapter, the control techniques employed in upper-limb soft-active exoskeletons are discussed to demonstrate their downsides and upsides. The mutual goal of the developed controllers is to adjust the exoskeletons' assistance level based on acquired sensory information from the human, which demonstrates his/her effort level. According to the state-of-art in this topic, usually, the EMG signal, or FMG (force myography) is fed to the controller as the input to detect the effort change of the user. Also, arm position is

considered in some works as the input to trigger the controller for a predefined repetitive task. As the output of the controller, the torque of the exoskeleton is adjusted to increase the support level, and eventually to reduce the effort at the targeted limb.

To begin with, in [70], a kinematic-based control is employed in an inflatable soft wearable robot (see Fig.1.1c) designed to support the shoulder of industrial workers for overhead tasks. The algorithm is developed based on shoulder and trunk kinematics. First, an onset angle (θ_{on}) is defined at the shoulder to detect the human intention to initiate the support. Also, the velocity of the shoulder ($\dot{\theta}$), and the trunk inclination angle (ϕ_i) are monitored as a part of the state machine. ϕ_{tol}, which is the tolerance threshold of the trunk, is determined to be 20°, and θ_{on} is assigned as 70° based on the targeted overhead task in the calibration season.

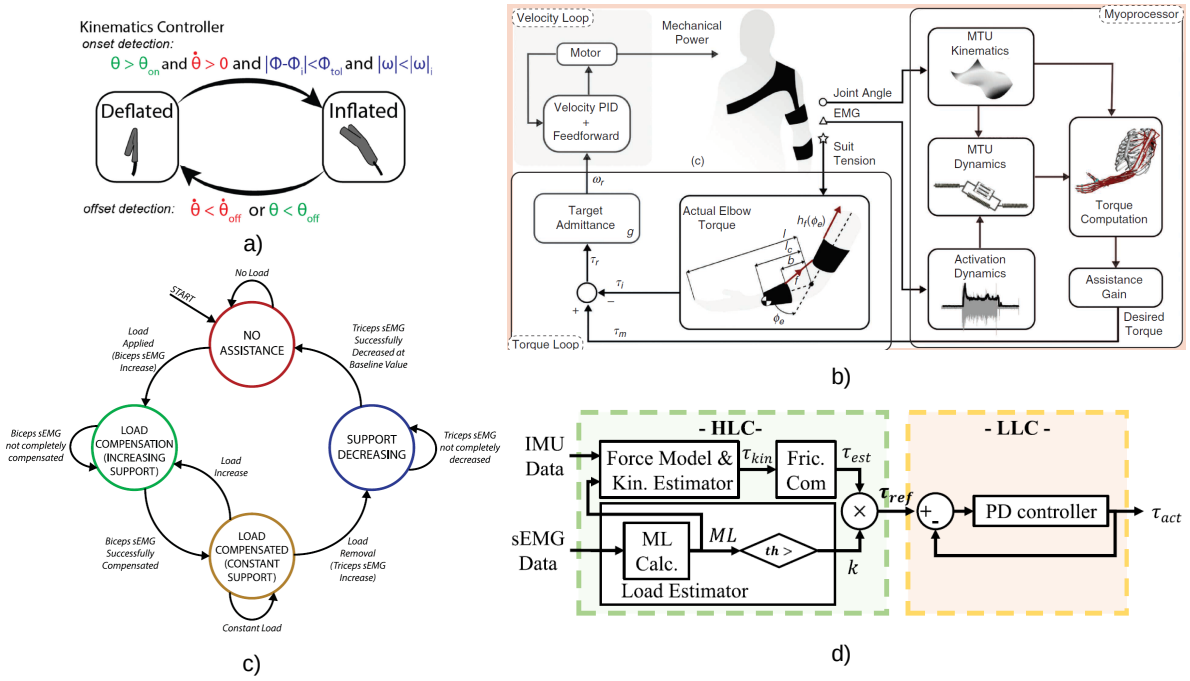

Figure 1.6: (a) A Kinematic-Based control state machine for a shoulder exoskeleton [44], (b) The control scheme of adaptive model-based myoelectric control for elbow assistive device [38], (c) The state machine of the load-compensation and load-release task for elbow exoskeleton [23], (d) The controller diagram of a shoulder exoskeleton [47].

In the working principle illustrated in Fig.1.6a, when the shoulder is i) above the θ_{on}, ii) $\dot{\theta} > 0$, iii) $\phi_i < \phi_{tol}$, the pneumatic textile actuator with bifurcated shape is inflated to counterbalance the shoulder. Instead, the aforementioned pneumatic textile actuator is deflated from the inflated state either the arm elevation angle is below the offset angle ($\theta_{off} = 60°$), or the arm extension velocity is above the offset velocity ($\dot{\theta}_{off}$). Therefore,

the human intention is perceived considering the kinematic relations of upper-body movements. However, the primary limitation of the system is to provide support in a short arm motion range (above the θ_{on}) because of the predefined specific task.

In another work [37], an EMG-driven control framework (see Fig.1.6b) is designed to control a soft elbow assistive device. The main motivation of the framework is to estimate the joint torque at the targeted limb based on i) three EMG channels including the long head of the biceps, long head of the triceps, and brachioradialis, ii) the elbow joint angle, and iii) a second-order muscle-twitch model which relies on nonlinear functions and musculoskeletal properties of the subject.

After acquiring the desired elbow joint torque through the above-mentioned methodology, the torque error is transferred to the joint velocity by making use of the admittance dynamics, and eventually, the resultant velocity is tracked by the DC motor. Although the response time of the developed technique is 53.8 ms, which is close to the physiological upper-limb electromechanical delay (55.5 ms), there is a long calibration season to identify the parameters of the developed model. A 3D motion capture system is utilized with markers attached to the metacarpus, lateral wrist, medial wrist, lateral elbow, medial elbow, and acromion. Then, the static pose acquisition, and maximum voluntary contraction are performed. Next, a generic musculoskeletal model is linearly scaled via OpenSim to be used for each subject's body. Finally, dynamic calibration is carried out by guiding the subjects through visual feedback that illustrates reference flexion/extension trajectories. Such long calibration intervals limit the applicability of the assistive device to ADL tasks. Moreover, although the load-compensation is achieved by making use of the designed framework, the load-releasing task is not carried out, which is crucial in repetitive ADL tasks such as pick and place.

In the next study, a control framework is developed to conduct both load-compensation and load-releasing operations using TSA based elbow exoskeleton (see Fig.1.4c). In the control interface shown in Fig.1.6c, first, sEMG sensors are placed on biceps and triceps muscles. For the load-compensation, when the load is held by the user, the EMG signal in biceps increases, and accordingly the support level is augmented by tensioning the strings in TSA. Contrary, when the load is released, the system cannot detect this state change and continues to provide assistance for the held load. Hence, the arm is pushed in an upward direction. At this moment, the user resists the exoskeleton to keep his/her arm in the same position, which increments the triceps contraction. This sudden effort change triggers the load-releasing state, and the exoskeleton reduces the support level to adapt the only forearm compensation. Even though the algorithm is tested under different payloads ($1-4$ kg) with both single and dual-arm on multi-subject, only a single

arm position is carried out in the experimental protocol. Moreover, such load-releasing strategy may disturb user's comfort and cause additional fatigue in the human joints for long term operations.

In another work, load-compensation and load-release operations are carried out using a control framework illustrated in Fig.1.6d for a shoulder exoskeleton developed for industrial tasks. For the former one, a Myo Armband is worn on the forearm to detect the overall activation level of forearm muscles using eight sEMG channels [47]. A threshold is assigned to introduce an effort level, and a constant muscle load gain is multiplied by the measured EMG channel data to measure the effort on the arm. When the calculated effort level is above the threshold, the torque is computed in the actuator to provide assistance. Otherwise, no support is provided to the user. For the load-releasing task, it is manually set in the torque control equation, which could be a limitation in dynamic tasks in industries. Moreover, the developed framework is tested at 3 specific arm positions on a single subject (see Fig.1.1b).

Finally, an FMG (force myography) based method is proposed to estimate the load level at hand by attaching force-sensitive resistors (FSR) on the upper arm for control of the upper-body exoskeleton [25]. According to the working principle, when the load is held at hand, the FSR is applied a normal force because of muscle contraction. Then, this action is detected by FSR, and post-processed, finally machine learning is conducted on the data to represent it in terms of the grasped payload. Even though the estimated payloads are close to the actual ones, the designed technique is tested at a static condition. Moreover, no method is mentioned for load-releasing tasks.

1.2.3. Goals and Contributions

In spite of the significant progress in the design of the soft-active exoskeletons, I believe that there is still a gap in the realization of an industry-fit wearable device for the elbow joint with the following characteristics: lightweight and cable-driven for better user-comfort, and shock-absorbing to protect both the actuation system and the wearer.

In view of the above requirements, in this thesis, I designed and developed a compliant exoskeleton for elbow joints using a series elastic actuation principle implemented by an endless shape elastic bungee element. This type of elastic element is selected due to its intrinsic damping, and compliant features similar to human muscles, which provide mechanical filtering against dynamic uncertainties such as impulsive forces, and oscillated movements because of possible controller issues.

The fundamental goal of the assistive device is to reduce the muscular effort of the user

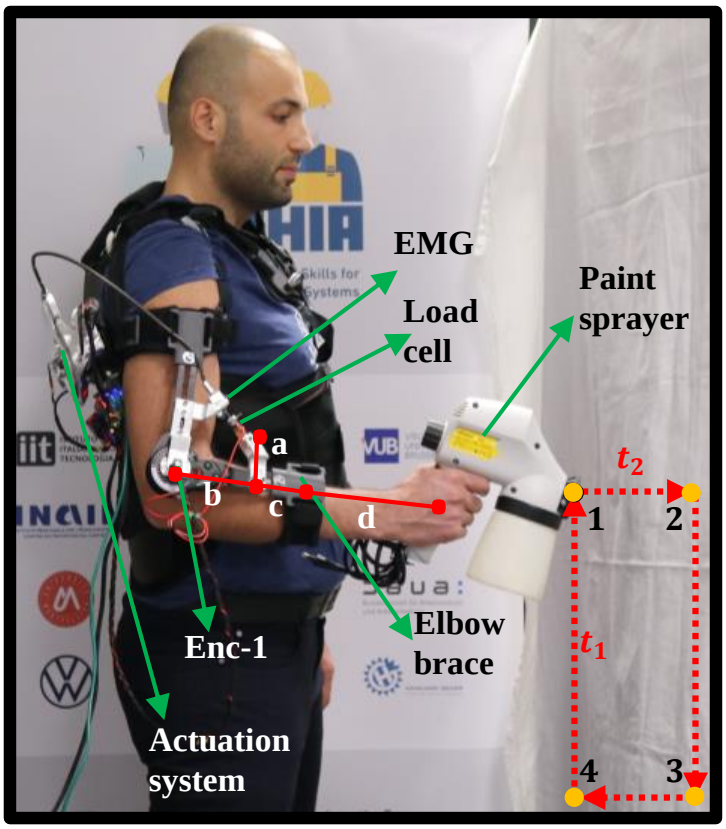

Figure 1.7: The developed compliant elbow effort-compensation device on S_1 (subject-1). t_1 and t_2 represent the completion time of the designed industrial test protocol for painting task. a and b are the fixed arm attachment distances whereas c and d are the adjustable arm distances for different subjects. Enc-1 is an encoder to measure the position of the elbow.

due to the internal (i.e., the forearm weight (2 kg in [6], [14]) and external (lightweight payloads (up to 1 kg)) loading. The main idea is to offload the user from a repetitive and prolonged exposure to load which can cause fatigue, and eventually reduce productivity in industrial applications. The prototype of the wearable system is illustrated in Fig.1.7. An actuation system is attached distally at the upper back of the user, while the generated force is transmitted to the human arm through a cable.

In summary, the contributions of this thesis is divided into two as part I, design and overall validation of the elbow effort-compensation device, and part II, adaptive control strategies for load-compensation and load-releasing operations. The part I contributions cover the authors' [A1], [A3], and [A4] publications in chapter-6, while part II is published in [A2].

The theoretical and practical contributions of part I are also reported separately. Theo-

retical ones are as follows :

- Sensitivity analysis of the assistive device to estimate the assistive force references to support different arm dimensions and forearm weights of users,
- Static force model of the new actuation mechanism with improved output force and working range,
- Introducing a new design methodology making use of the static force analysis of the device, and accounting for the actuation systems' parameters (i.e., bungee force model, spool mechanism dimensions, etc.) to select the optimized machine elements including ball-screw,
- Damping ratio index estimation of the assistive device to mathematically prove its intrinsic compliance characteristic,
- Power analysis of the assistive device with max payload (4 kg) under position control on a benchtop setup at different frequencies and repetitive motions.

Practical contributions are reported below:

- Proof-of-concept prototype of the assistive device's actuation system,
- Design and development of the actuation system with improved output force and working range,
- Development of a wearable support device based on the actuation system,
- Vibration isolation performance of the assistive device under position control at high-frequency cyclic movements on a benchtop setup with and without bungee elastic element through FFT analysis,
- Validation of the shock-absorbing ability of the system on a benchtop setup with and without bungee element under impact force,
- Designing an industrial test protocol with long-term operations, and testing the device on 6 subjects at high-velocity movements under human-in-command movement control (force control), with and without assistance.

Regarding the part II contributions, I focused on control challenges of soft-active ADL exoskeletons. As previously mentioned in 1.2.2, although several control strategies are developed for wearable devices to generate assistive torque based on EMG sensors, the load release phase has not been studied in the literature according to my knowledge. To clarify, the research question I address in part II contribution is when an object is released from

the hand, how the assistive force reference of the exoskeleton can be adapted intuitively to the new payload (i.e. only arm compensation) without disturbing users' comfort?

To begin with, the device is controlled in force to enable movement transparency and to enhance user comfort when carrying external loads. The force reference is formed by the forearm weight and the load at hand, with the latter being detected and compensated online through an EMG based adaptive method. To do so, an assistive force is generated when the EMG of the biceps muscle goes above a threshold determined according to the user's muscle contraction under forearm compensation support. Subsequently, as soon as the EMG settles below this threshold, the load at hand is estimated based on the position of the elbow, the tendon force, and the geometry of the arm attachments.

Since the exoskeleton is controlled in force, sudden load release or similar disturbances may result in rapid device movements due to the feed-forward compensation forces, undermining users' safety. Hence, I propose and implement a power-aware control algorithm to decouple the load-related assistive forces from the controller. To achieve this, the power of the exoskeleton is calculated during the operation according to the weight of the user's forearm, the target payloads at hand, and the cable velocity. Next, a power threshold is assigned based on the user's cyclic motions. When the load is released from the hand, the power of the device increases suddenly above the threshold, and the external proportion of the reference load is eliminated. Hence, the exoskeleton will switch back to compensating the forearm weight and the user can comfortably move the own arm without interrupts.

In summary, the part II contributions of the thesis is presented below:

- Development and experimental verification of the power-aware control strategy to perform fast and smooth force adaptation to object releasing phase on a benchtop test with different payloads, different speeds, and different releasing positions,
- Development of the load compensation algorithm using biceps EMG sensor output, and experimental validation of the load compensation and release algorithms on eight subjects for two different payloads at different elbow angles, and performance evaluation in terms of compensation/release time, and effort reduction with respect to non-powered exoskeleton case.

1.2.4. Outline

The graphical abstract, and the overview of the thesis is illustrated in Fig.1.8, and 1.9, respectively. In chapter-2, the design methodology is explained starting from the velocity, and motion range of the elbow in view of the industrial use cases of SOPHIA European

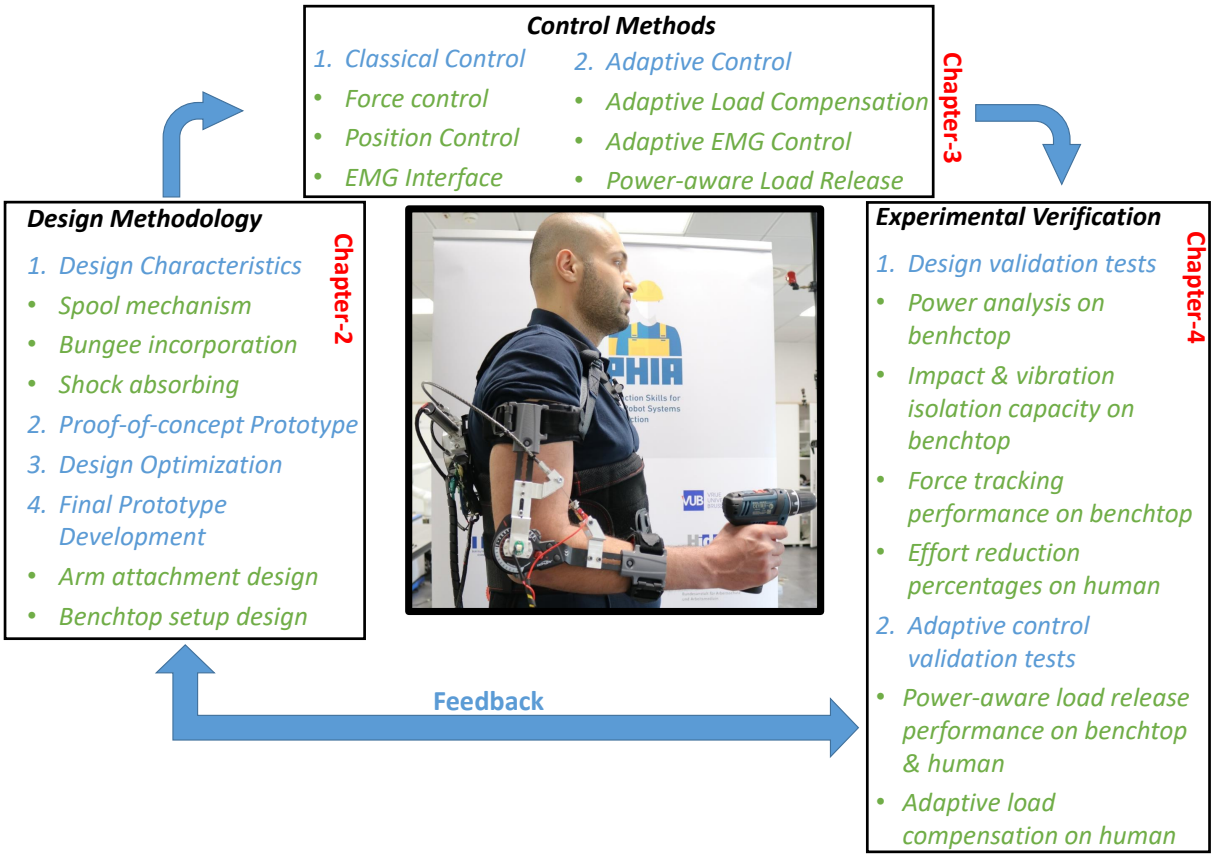

Figure 1.8: The graphical abstract of the thesis.

project. Next, the maximum torque is computed by making use of the force analysis derived with the help of the geometry of the arm attachment, and the maximum payload at hand. Then, the elastic element determination is carried out to perform series elastic actuation strategy. A bungee, which has a damping feature, is incorporated into the mechanism to intrinsically isolate the vibrations, and sudden impacts similar to human muscles. Afterward, a spool mechanism concept is studied to maximize the elastic force and to wrap/release cable during the operation. Accordingly, the static force analysis is conducted for the aforementioned mechanism to compute the desired bungee force. Later on, a proof-of-concept prototype is developed through 3D printing technology to monitor the motion and force range of the device under fixed-end and open-end experiment conditions. Moreover, a couple of limitations are detected on this functional prototype to be optimized for the final prototype such as stretching and bending issues of some parts. Therefore, fundamental modifications are applied to the new design to overcome those challenges. In addition, a computation methodology is carried out in the selection of the design parameters of this final prototype. Then, the machine elements including the motor and ball screw are chosen by taking into account the desired motor torque, and

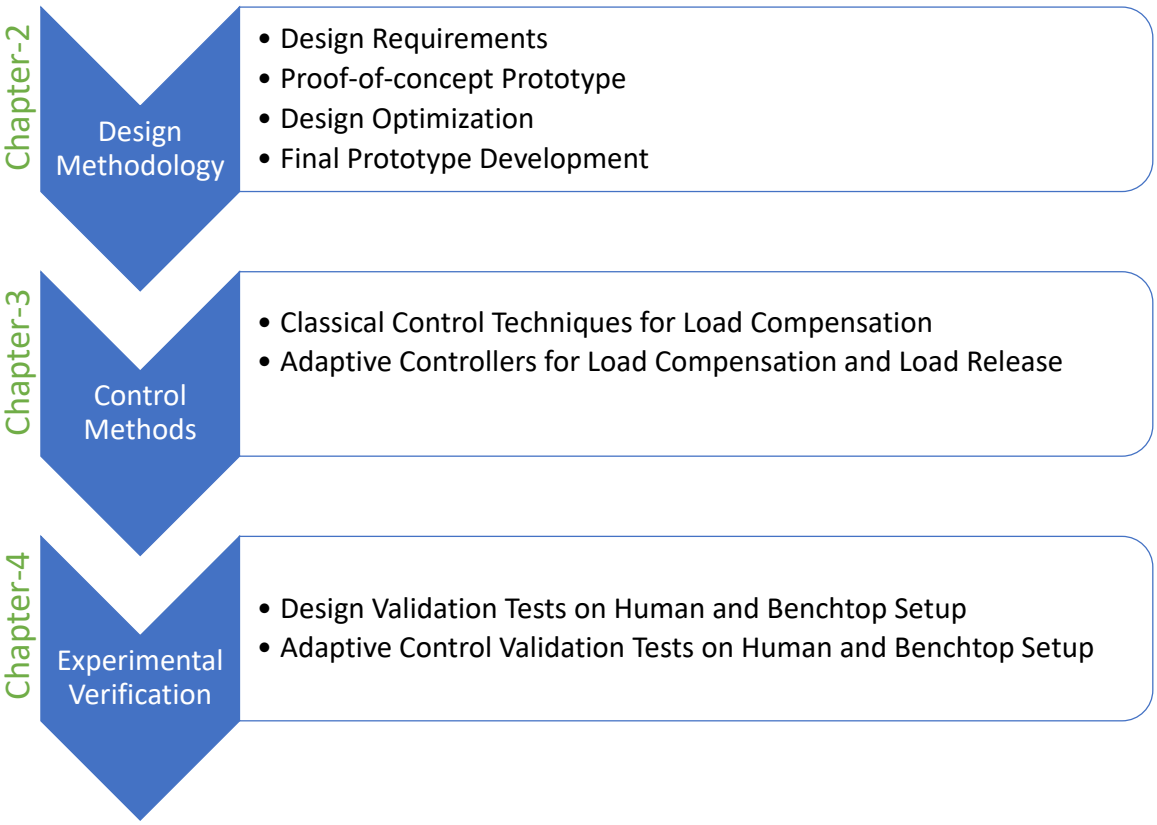

Figure 1.9: The graphical overview of the thesis. Chapter-2 aims to introduce the design methodology based on the design requirements, functional prototype development, design optimization, and the final effort-compensation device. Chapter-3, and 4 are organized to express control techniques, and their validation, respectively.

velocity. Finally, finite element analysis (FEA) simulation is performed on the critical parts to evaluate their displacement under the computed maximum elastic force, and then the design of the arm attachment and benchtop setup is expressed to build a wearable support device based on the developed actuation mechanism.

In chapter-3, several performance metrics on the control of the device are determined to increase the wearers' comfort in terms of high effort reduction and fast adaptation to load changes at hand. In light of those goals, classical and adaptive control techniques are studied. The former is adapted to verify the performance of the design through simple PID-based position and force control. To clarify, the idea is to validate the motion range, force tracking and effort reduction performance, energy analysis, and intrinsic vibration and impact absorption characteristics of the mechanism. Also, the sensitivity analysis is studied to compute the input force references for multi-subjects with different forearm specifications such as forearm weight, and a couple of geometric terms illustrated in Fig.1.7

(c, d). Later on, adaptive control strategies are fulfilled to automatically detect the load change at hand through the EMG sensor attached to the biceps muscle. Moreover, the load releasing action is achieved with the help of the power-aware control strategy.

In chapter-4, a number of experimental protocols are contemplated to assess the performance of the device. The experiments are divided into two sections. The first one is introduced as the design validation tests, which aim to demonstrate the previously mentioned features of the mechanism (i.e., torque, motion, and velocity range, intrinsic compliance etc.) through classical controllers, that is, PID-based force and position. Moreover, the experiments are carried out on both the benchtop and humans with the former decoupling the human compliance to show only the intrinsic compliance and the energy consumption of the mechanism. Afterward, an equivalent industrial painting task is designed to evaluate the device on 6 subjects with different forearm specifications under force control implemented for 5 minutes of continuous operation. Finally, the before-mentioned adaptive controllers are tested to verify the derived control equations on 8 subjects with different payloads, velocities, load compensation, and releasing arm positions.

In chapter-5, the prominent results of the developed effort-compensation device are reported, and the possible future developments are discussed.

2 | Design of the Elbow Effort-Compensation Device

The focus of this chapter is to explain the design details of the assistive device. First, a maximum payload at hand, motion, and velocity range of the wearer are assigned based on an industrial use case. Next, the torque and kinematic formulations of the device are derived to compute their maximum values. Then, a bungee elastic element is selected to carry out series elastic actuation principle, and then spool mechanism alternatives are explained in view of a bunch of design requirements. Afterward, static force analysis of this mechanism is studied to compute the desired maximum bungee force, which has a fundamental role on the mechanical design of the actuation system of the assistive device.

In the next step, a proof-of-concept (POC) prototype is built to explain the general concept of the proposed assistive device, and the preliminary experiments of its actuation mechanism (motion range and output force profile), which is tested on a plastic elbow produced by mimicking the human arm dimensions. After verifying the working principle practically, certain design limitations are detected in the POC prototype, and necessary modifications are applied to the improved prototype.

Consequently, the mechanical design of the final actuation mechanism, arm attachments and the benchtop setup are fulfilled. Also, a computation methodology is developed making use of the static force analysis of the device and taking into account the actuation system parameters including the bungee force model, and spool mechanism dimensions to opt for the optimized machine elements such as ball-screw and motor. Finally, the finite element analysis (FEA) is carried out to validate the strength of the critical parts under the maximum calculated bungee force thanks to the static force analysis.

In summary, a methodology is studied considering the following steps:

- the torque and motion range of the elbow,
- elastic element determination,
- spool mechanism design approach,

- static force analysis of the spool system,
- the proof-of-concept mechanical design, and preliminary tests,
- the optimization of the mechanical design,
- the choice of the design parameters based on a computation methodology,
- the selection of the machine elements including motor and ball-screw,
- the FEA simulations of the critical parts,
- the mechanical design of the arm attachment, and the benchtop setup.

2.1. Torque and Motion Range of the Elbow

The first input of the design methodology is to determine the desired elbow velocity and the motion range that the assistive device can provide. This information is acquired considering the industrial use-case of the European project SOPHIA. In that, 4 screenshots of the workers movements are presented in Fig.2.1, and the elbow motion range and the velocity are assigned to be $80°\pm5°$, and $25\pm5°/s$, respectively. Therefore, the upper-limits are $85°$ (θ_{max}), and $30°/s$ (V_{max}).

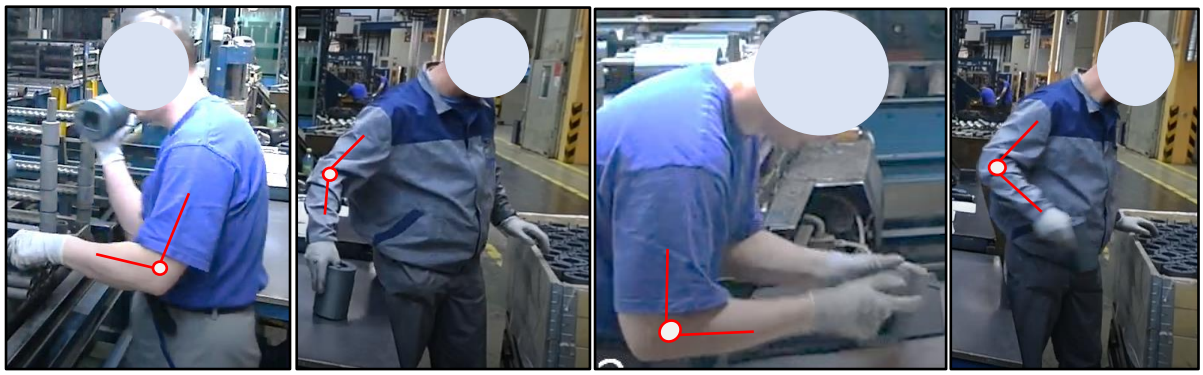

Figure 2.1: The screenshots of the industrial use-case of the European project SOPHIA. Max elbow position is $\theta = 80°\pm5°$.

Afterward, a diagram is drawn in Fig.2.2 which illustrates the general concept of the actuation mechanism and the arm attachments. Starting from the latter one, in our calculations, the elbow joint is assumed as a single-axis hinge joint, with its axis being symmetric with respect to both upper and lower limbs according to the human model mentioned in [50], [26]. Also, a compliant elbow brace, shown in gray color in Fig.2.2B, is used to achieve a compliant coupling with the arm. As mentioned previously, the

generated assistive force in the actuation mechanism is transferred to the brace through the Bowden cable shown in red dashed lines in Fig.2.2B.

There are some parameters including a, b, c, d in mm, and $\phi, \alpha, \beta, \gamma, \theta$ in radian. To clarify, a and b are the fixed attachment distances while c can be varied mechanically thanks to the design, which also changes the d. $(b+c)$ represents the center of mass of the forearm, and it is utilized in the calculation of the elbow joint torque. The average value of anthropomorphic c/d values are 50/150 mm based on [14],[6], which means the center of mass of the forearm is measured as the middle point in between the elbow center of rotation and the hand. Since this c/d can be changed from one person to other, it is designed adjustable to achieve adaptation to multi-subjects.

According to the design concept, a max payload 1 kg (W_L) is held by a human based on the SOPHIA industrial use-case, and W_a is the forearm weight (20 N based on [6]). The desired torque at O_3 can be calculated as follows:

$$\tau = \overbrace{W_L \sin(\theta) l_L}^{\tau_L} + \overbrace{W_a \sin(\theta) l_a}^{\tau_A}, \tag{2.1}$$

where l_a, and l_l are the lever length for the arm $(b+c)$, and the load $(b+c+d)$, respectively.

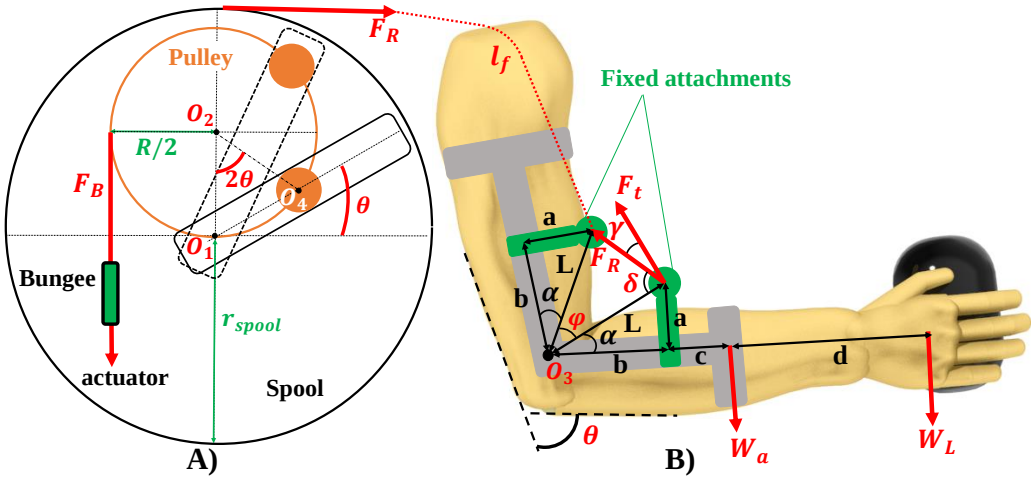

Figure 2.2: The illustration of the working principle of the actuation system (A) and the arm attachments (B). The dashed red line represents the Bowden cable that transfers the generated elastic force in the actuation system to the arm while roller is illustrated in orange. The vertical distance between elbow brace (shown in gray color) and first anchor point on the forearm (a), the distance of fixed attachments from O_3 (b), the center of mass of the forearm (b+c), and the lever arm (b+c+d) from the external load (W_L) to O_3.

Table 2.1: Target values for design performance

Motion range (θ_{max})	85°(80 ±5)
Desired velocity (V_{max})	30 deg/s (25 ± 5)
Desired torque (τ) / Cable force (F_R)	6.8 Nm / 65 N
Mass	as light as possible
Spool and pulley diameter (R, r_{spool})	40 mm and 85 mm
Ball-screw stroke (S) / Cable length (l_f)	80 mm / 119 mm
Fixed attachment distances (a, b)	50 mm, 100 mm
Max variable arm distances (c, d)	70 mm, 170 mm

Moreover, the maximum applicable values of c, and d are reported in Table.2.1. Accordingly, the necessary cable force to generate this torque support is computed in (2.2), and reported in Table.2.1.

$$F_R = \frac{\tau}{L\cos(\gamma)}, \quad \gamma = 90 - \alpha - (\theta/2), \quad \alpha = \arctan(a/b), \quad L = \sqrt{a^2 + b^2}. \tag{2.2}$$

Moreover, F_R can be written out as the summation of F_A and F_L, in which the former represents the force reference for the arm support, and the latter is for the external loads. By substituting $\tau = \tau_A$, and $\tau = \tau_L$ in (2.2), those force references are computed as follows:

$$F_L = \frac{W_L \sin(\theta) l_L}{L\cos(\gamma)}, \qquad F_A = \frac{W_a \sin(\theta) l_A}{L\cos(\gamma)}. \tag{2.3}$$

Finally, the required cable length is calculated at approximately 119 mm using (2.4) to perform flexion/extension movements in the range of the θ_{Max}.

$$l_f = \sqrt{2(a^2 + b^2)(1 - \cos\varphi)}. \tag{2.4}$$

2.2. Elastic Element Determination

As the next step, an elastic element is incorporated in the actuation/transmission of an elbow assistive device considering two reasons. First, it provides an intrinsically softer interaction between the actuation system of the device and the limb of the human body where the actuation output is applied. In this way, the force transmission from the

assistive device to the human body can be accomplished in a compliant way. Another advantage is that, such an elastic element eventually forms a mechanical filter against dynamic uncertainties absorbing sudden motions or possible control issues and protecting both the actuation of the device as well the human subject from feeling such dynamic force transients.

Important to note that if there was no damping feature in human muscles, it would not be possible to change the position of a limb accurately and quickly, and tackle with the impulsive forces [32, 40].

Figure 2.3: The illustration of the endless type bungee with diameter 10 mm (a), and 5 mm (b).

Considering the above reasons, an endless shape bungee cord (see Fig.2.3), which is made of rubber, is selected as the elastic element, and its elongation is regulated through an actuator, that is, a ball-screw and a DC motor. The reason for the endless shape bungee is due to its intrinsic damping feature, lightweight property, and elongation capacity, which is more than a metal spring. Also, there are several performance properties such as a number of configurations alternatives (i.e., endless and U shape [58]), eliminating the need for end-fittings for the assembly. For instance, the bungee shapes illustrated in Fig.2.3 are produced specifically based on our needs by the company. The target is to reach the desired stiffness with the shortest bungee elongation to have a compact, yet powerful mechanism design.

2.3. Spool Mechanism Design Approach

In the next step, the spool mechanism, which is connected on one side with the elastic element and on other with the human arm, is developed considering three criteria.

- The mechanism should wrap/release the computed cable length (l_f) during the flexion/extension movement of a human forearm.
- The mechanism shall transfer the generated bungee force to the wearer throughout the targeted elbow motion range.
- It is aimed to achieve a 1:1 motion relation between the spool mechanism and the elbow during the flexion/extension movements to avoid multiple coiling on this mechanism, which usually leads to adding an extra clutch and the feeder system to tackle the cable slack and guiding [7].

Towards achieving those objectives, two different spool systems are considered, and presented in Fig.2.4. As a first alternative, shown in case-1, if a pulley and a spool are placed at the same axis (O_1), and the bungee is connected with the pulley, the bungee force is multiplied by the ratio of the pulley and the spool radius. Instead, if the center of the spool and the pulley are separated as illustrated in case-2, the bungee force is multiplied by the ratio of the diameter of the pulley and the spool radius, leading to having twice as much bungee force as the first alternative. Therefore, the latter approach is selected, and its detailed force analysis is explained in the next section.

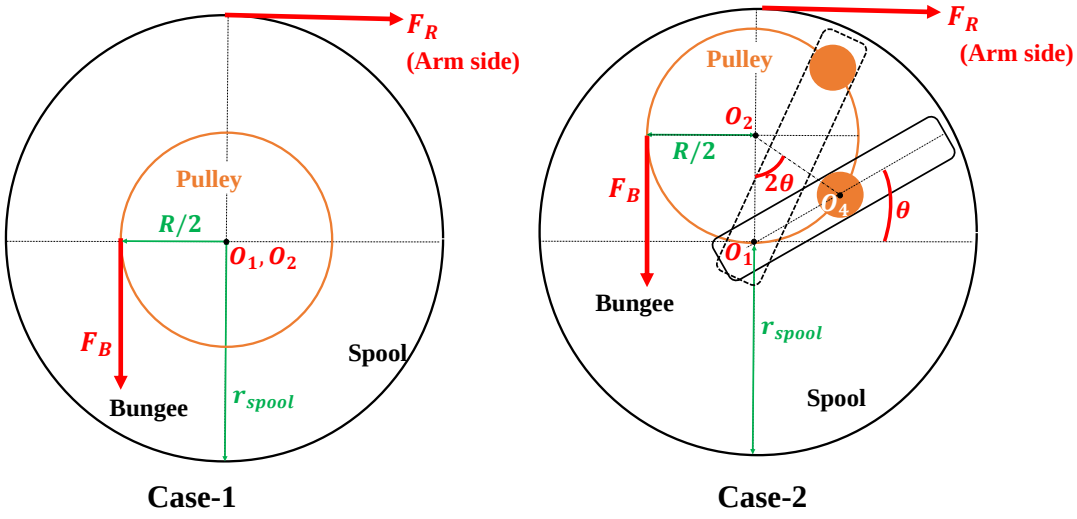

Figure 2.4: The spool system alternatives. Case-1 represents the spool design in which the pulley and spool are placed co-axially. Instead, case-2 illustrates the spool design where center of the pulley (O_2) and the spool (O_1) is separated.

Regarding the working principle, the pulley is connected with the bungee to create an input torque around O_2. Also, a roller (see Fig.2.2) is attached to this pulley. Next, a slot is opened in the spool, and the roller is mounted on it. For instance, when assistance is needed, the DC motor regulates the elongation of the bungee, and then the elastic force is

transmitted to the spool with the help of the roller. Also, this element can slide inside the slot to make the spool perform the same amount of rotation with the elbow [42]. Finally, the elastic torque on the spool is transmitted to the human arm with the help of a tendon cable.

2.4. Static Force Analysis of the Spool System

After selecting the spool mechanism, its static force analysis is carried out to formulate the bungee force as a function of the mechanism dimensions. To do that, all the forces acting on each element are taken into account, and illustrated in Fig.2.5. Starting from the pulley, bungee force (F_B) is acting around 0_2, and there is a reaction force (F_{reac}) at the contact point (O_4) between the roller and the slot opened in the spool. Therefore, the moment equilibrium is written out around O_2 as follows:

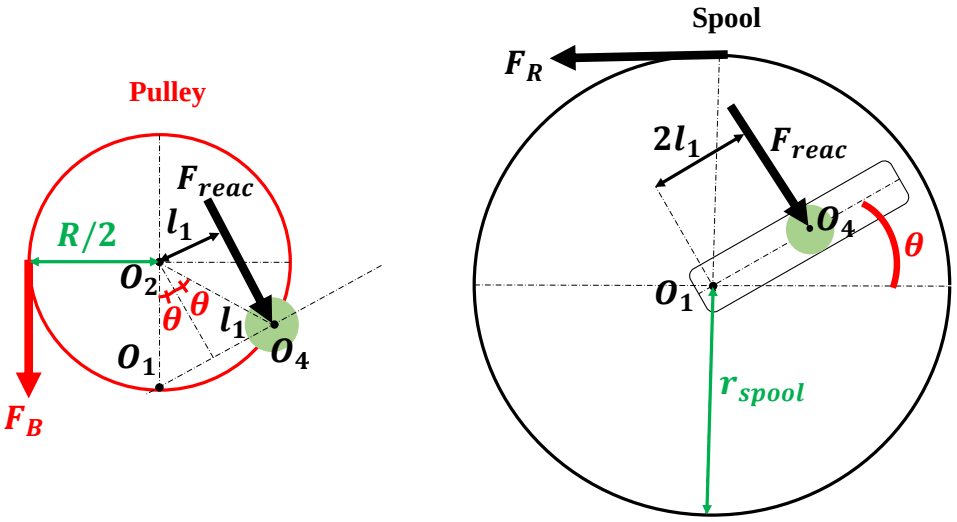

Figure 2.5: The illustration of forces acting on the spool and the pulley.

$$(F_B)(R/2) = (F_{reac})(l_1) \quad \rightarrow \quad F_{reac} = \frac{F_B}{\sin\theta} \tag{2.5}$$

where l_1 is $\left(\frac{R}{2}\sin\theta\right)$. Next, the calculated F_{reac} is transferred to the spool element, and the moment equilibrium is written about O_1. Hence:

$$(F_R)(r_{spool}) = (F_{reac})(2l_1). \tag{2.6}$$

By substituting F_{reac}, and l_1 in (2.6), and isolating F_B, following equality is acquired:

$$F_B = \frac{\overbrace{(F_R)(\sigma)}^{F_D}(r_{spool})}{R}, \tag{2.7}$$

where σ represents the safety factor, which is assigned as 1.3, to compensate the possible slip on the human arm attachments, frictions in the actuation system, possible manufacturing errors and backlashes. Therefore, from now on, the desired bungee force (F_B) is taken into consideration with the safety factor.

As mentioned in section 2.3, two spool system is compared. Just to mathematically prove why case-1 is not selected for the design, the moment equilibrium is written about O_1, O_2 for case-1 shown in Fig.2.4. Thus:

$$(F_B)(R/2) = (F_R)(r_{spool}) \quad \rightarrow \quad F_B = \frac{F_R(2)(r_{spool})}{R}. \tag{2.8}$$

Comparing (2.7), and (2.8), it is clear that the latter requires double bungee force than that of former, leading to have a greater actuator, and machine elements. This concludes that case-2 has a better force transmission characteristic then case-1.

2.5. The Proof-of-Concept Prototype

Before moving to the further steps, the functionality of the proposed elbow device is tested in two different experiments including fixed-end (elbow-1) and open-end (elbow-2) by making use of the two 3D printed elbow prototypes (see Fig. 2.7).

2.5.1. Mechanical Design

The assistive device structure is divided into two sections, the power unit, and the spool system in Fig. 2.6. The power unit aims to generate an elastic force to be transferred to the spool system as an input. To achieve this, a Maxon brushless DC motor (EC-4pole 22, 323218) with 5.4 : 1 gearbox is coupled with a ball-screw mechanism to move the plate component linearly. An endless ring type of bungee (thickness ϕ 5 mm and initial length 55 mm in Fig.2.3b) mounted on two supports is connected with the pulley through the Bowden tendon.

In the spool system, a roller, which slides inside the spool, is coupled with a pulley to vary the input elastic force. However, based on the working principle of the spool and the pulley in Fig. 2.2A, there is a challenge to rotate the spool for small angles. For instance,

Table 2.2: Design parameters of the proof-of-concept prototype

R (mm)	θ_{max}	r_{spool} (mm)	S (mm)
40	116°	88	100

if a normal shaft is coupled with the spool rotation axis (O_1) for the bedding purpose, the roller will not be able to approach to O_1 more than the diameter of this shaft. To address this issue, an eccentric shaft is developed not only for the bedding purpose of the spool but also for allowing the roller to approach O_1 at the small angles (see Fig. 2.6). With this new part, the operating range of the elbow and the spool is optimized to be between $\approx 9 - 116°$. In addition, a flange is designed and assembled from the upper side to align the spool and eccentric shaft on the same axis.

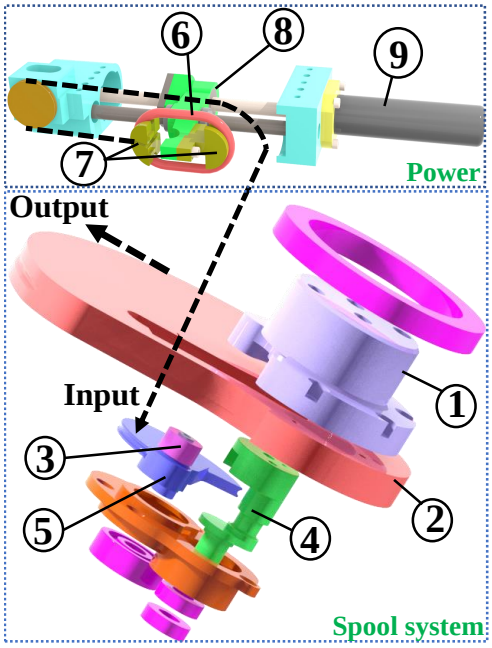

Figure 2.6: Mechanical design of the POC prototype. 1- Flange, 2- Spool, 3- Roller, 4- Eccentric shaft, 5- Camshaft, 6- Bungee, 7- Supports, 8- Plate, 9- Motor.

Finally, elbow-1 is fabricated and illustrated in Fig. 2.7 considering the human forearm dimensions and the location of the fixed attachments (see Fig. 2.2). Several holes are opened on this plastic elbow with 15° resolution to measure the torque variation in 7 test angles.

Regarding the open-end experiment, elbow-2 is manufactured, and an encoder is attached to this elbow (see Fig. 2.7). Another encoder, which is not illustrated in Fig.2.6 to reduce the complexity, is coupled with the flange part to compare if spool and elbow-2 achieve the same rotations.

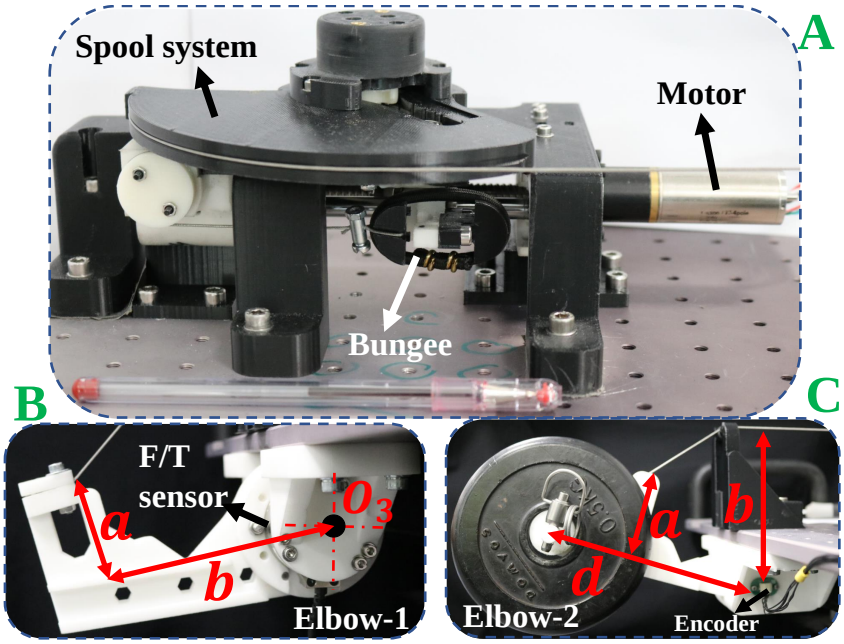

Figure 2.7: The illustration of the 3D printed assistive device. A) Cam-spool system and power unit. B) Fixed-end experiment C) Open-end experiment

To calculate the spool radius and the ball-screw stroke, two design parameters are assigned in Table.2.2 for the diameter of pulley (R) and the working range of the elbow (θ_{max}). Even though θ_{max} is introduced to be 80°±5° earlier for the targeted use-case (see Table.2.1), it is assigned over the desired value for POC prototype to monitor the actuation mechanism in a wider motion range. Using these parameters, the spool radius is computed as follows. Hence:

$$r_{spool} = \frac{l_f}{\theta_{max}}. \tag{2.9}$$

Additionally, the tendon length wrapped around the pulley is calculated to determine the necessary stroke in the ball-screw transmission of the power unit. Therefore, the ball-screw stroke is calculated as follows:

$$S = (2\theta_{max})(R/2). \tag{2.10}$$

Considering an additional 20 mm tolerance for the elongation of the bungee, the ball-screw stroke is selected as 100 mm (see Table.2.2).

2.5.2. Experiments and Results

Two experiments under fixed-end and open-end conditions are carried out using a 3D fabricated prototype (see Fig. 2.7) and presented in this section. In the first experiment, the elbow-1 is coupled rigidly with an F/T sensor (ATI-Mini45, SI 145-5), and they are both fixed to a table through apparatus. Center pins and screws are used to engage the elbow-1 and F/T sensor so that the applied assistive device force can be measured in different test angles. In the open-end experiment, the elbow-2 is free to rotate, and the aim is to measure the motion range of the assistive device.

A motor driver and a data acquisition card communicating through EtherCAT at 1kHz is used to control the assistive device. A PID regulator is used through MATLAB®/ Simulink Real-Time interface to drive the motor in power unit. The resultant linear position error on the ball-screw mechanism is detected between ±0.15mm. Additionally, a 0.5 ± 0.1 Nm bias torque is maintained with the help of the assistive device in the fixed-end experiment to avoid relaxation on the cable and compensate for any backlash in the assembly.

Fixed-end

In this test, first, the spool mechanism is decoupled from the actuation system, and only the power unit is connected directly with the plastic elbow-1. The force profile of the bungee is evaluated by tensioning the bungee between $0-10$ mm (0.5 mm position increment) in each predetermined elbow test angle ($15^\circ - 105^\circ$) and measuring the resultant torque around O_3 at elbow-1. These data are substituted into (2.2) as τ, and the estimated force profiles, that is the tendon force (F_R), are illustrated in Fig. 2.8. Furthermore, the average values of those estimated forces are calculated for each pretension value, and the resulting shape is demonstrated as “average" in the same figure. Finally, the same bungee is elongated (similar pretensions as elbow-1) using another tension machine. The measured force profile are reported as “desired" in the same figure.

According to the results in Fig. 2.8, the force profiles slowly rise in the beginning, then the trend sharply increases until 4% elongation, while for larger elongations the slope of the increment reduces. It is obvious that the differences in the force shapes among the test angles are insignificant, which indicates that the assembly of the components, cable connections and the force estimation based on (2.2) are achieved with minimal error. There is also an almost constant shift between desired and average force curves in most of the entire pretension points. This originates from the uncertainties of the plastic parts, such as stretching, manufacturing errors, as well as the friction in the cable.

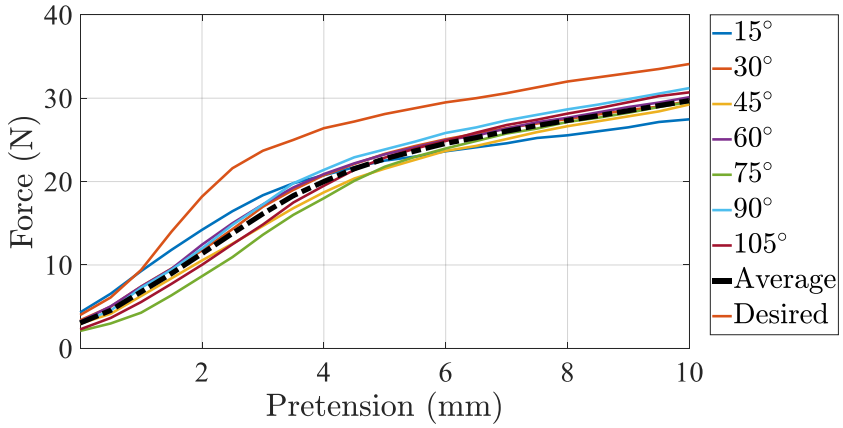

Figure 2.8: Stiffness profile of an endless ring type of bungee (thickness ϕ 5 mm and initial length 55 mm).

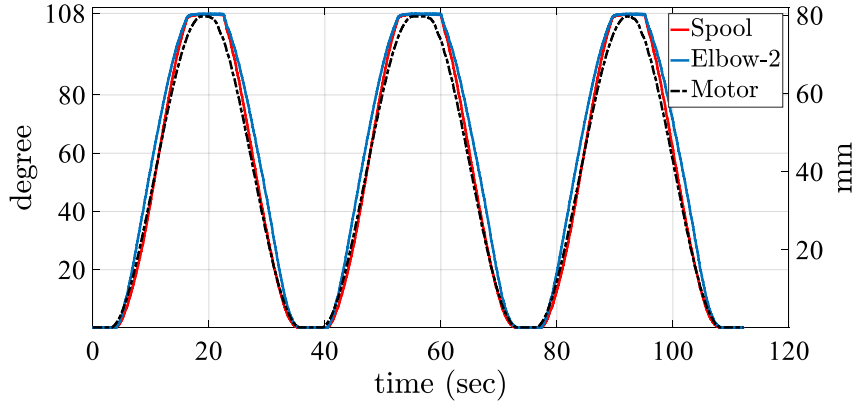

Figure 2.9: The results of the open-end experiment. The right and left vertical axes illustrate the angular and linear position changes, respectively.

Next, the actuation system (i.e., power and spool system units) is tested to acquire the output force profile of the actuation mechanism. To implement that, first, the desired torque profile, which is expected to be delivered by the assistive device, is calculated by substituting 5N for W_l in (2.3). Then, the elbow-1 is configured and fixed mechanically in all the test points ($15° - 105°$) one by one, and the spool is rotated through the motor to the same position as that of the elbow-1. Subsequently, the bungee is tensioned, starting from 1 to 10 mm (1mm position increment) with the help of the motor in each test angle. Every pretension is repeated three times (standard deviation $\approx 0.1 - 0.0006$). Finally, the average values of those data are extracted from the bias torque, and presented in Fig.2.10. It is clear that the S-shape profile of the bungee is slightly changed due to

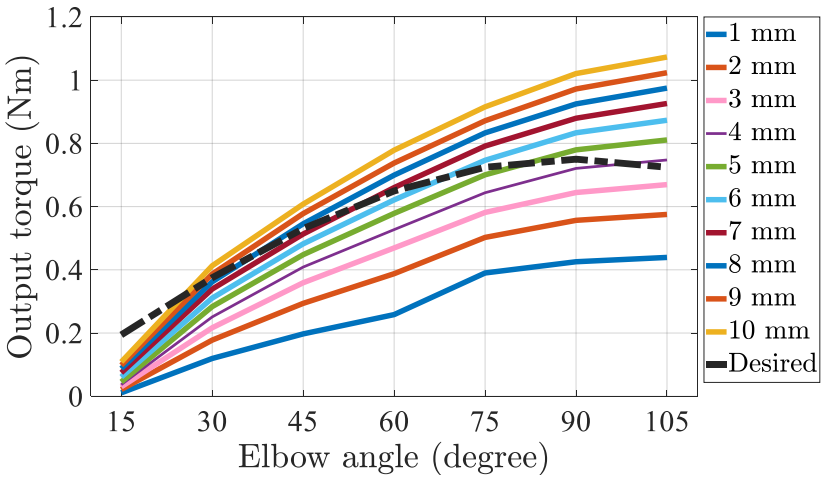

Figure 2.10: Measured torque results of the fixed-end experiment, and the desired torque curve to balance 5N load in the forearm.

the nonlinear effects of the spool mechanism such as frictions, backlashes and stretching. Also, the targeted payload (W_l = 5N) can be balanced according to the acquired force trends. These preliminary results gave solid evidence on the validity and utility of the proposed design concept.

Open-end

In this test, a 0.5 kg load is mounted on the elbow-2, and the motor is driven to achieve the selected ball-screw stroke (see Table.2.2) for the flexion and extension movement. It can be seen in Fig. 2.9 that the position difference between the spool and the elbow is very low (RMS = 6.14°), which validates the proposed design concept. In addition, the measured angular position data verify the targeted kinematic working range of the elbow, which varies between $9 - 116°$ ($\approx 108°$). Note that, the 9° shift in the spool position is not visible in Fig.2.9 as the encoder is initialized at its minimum position. That angle is acquired from the CAD file of the mechanism.

2.6. Optimization of the Mechanical Design

In this step, first, the drawbacks of the POC prototype is discussed, and the necessary modifications are carried out to improve it. The detected limitations are expressed below.

- Since the diameter of the spool is sharply greater than the eccentric shaft (see Fig.2.6), the bending is unavoidable under the tangential force on the spool.
- The vertical distance between the spool excitation diameter (i.e., the cable guide)

and the bearings for its bedding is ≈ 25 mm since the spool is assembled on the top of the eccentric shaft. Hence, this causes an increase in the bending force, and the problem is solved by increasing the size of the parts since the idea is only to validate the functionality of the system on a table test bench.

- The working range of the spool (i.e., motion range of the elbow) is also constrained due to the working principle of the spool and the eccentric shaft.

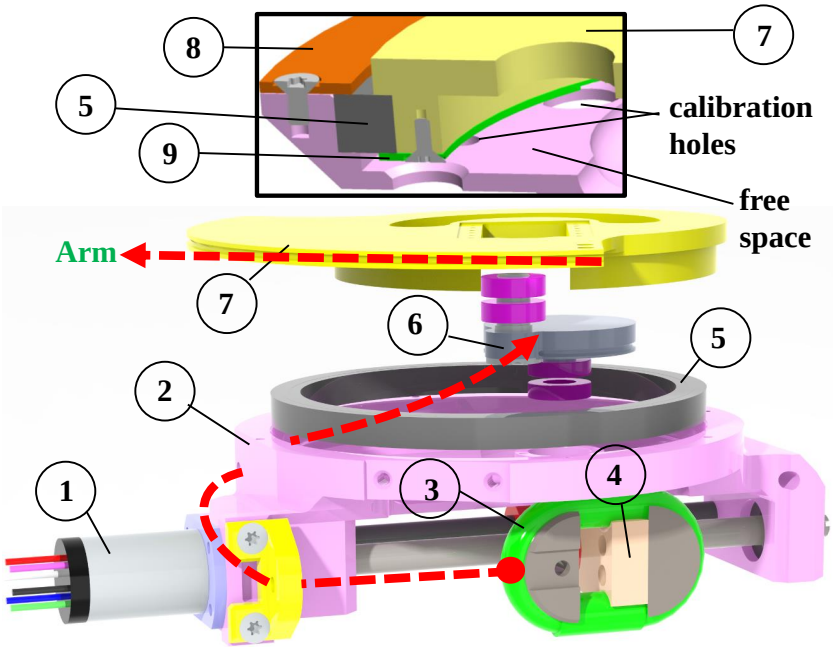

Figure 2.11: Mechanical design of the actuation system. 1- Motor, 2- Base, 3- Bungee, 4- Plate, 5- Spool bearing, 6- Pulley, 7- Spool, 8-Flange-1, 9-Flange-2. Tendon cable is illustrated with red dashed lines.

To begin with, similar to the POC prototype, the mechanical design of the actuation system is explained by dividing it into two sections as power, whose components are 1,2,3,4, and the rest constitute the spool mechanism (see Fig.2.11). For the former, a DC motor is coupled with a ball screw, which is assembled to a plate to change the elongation of the bungee as well as a wrap/release the tendon cable on the pulley during flexion/extension movements. All these components are fixed on a single base to have a compact and robust structure. Later on, this generated elastic force is transmitted to the spool mechanism, and subsequently to human arm attachments through the tendon cable.

Reexamining the previously mentioned limitations of the POC mechanism, in the new design, a fundamental modification is implemented on the bedding of the spool considering the three criteria stated here.

- The spool is supposed to be bedding directly to the base with a lightweight and compact bearing without interfering with the pulley and the roller.
- The working range of the spool shall be either the same as the previous design or enhanced.
- The height of the spool mechanism should not be increased more than the previous prototype [42] so that the resulting structure is not bulky.

Focusing on those objectives, a bearing (defined as spool bearing in Fig.2.11) is used in the bedding of the spool to the base while allowing the pulley to perform its motion without any interference with the inner diameter of the spool bearing. To clarify, first, flange-2 is put on the free space inside the base. Then, the spool bearing is assembled with the spool, and both of them are placed on the base (see section view in Fig.2.11). Next, flange-2 and the spool are coupled using the calibration holes that are opened on the base to align the spool and flange-2 holes for assembly purposes.

Finally, flange-1 is placed on top of the spool bearing and fixed on the base as an upper shoulder. In this way, while flange-2 rotates together with the spool bearings' inner ring, flange-1 is fixed on top of the spool bearing to keep the spool bearings' outer ring stationary. In this way, since the spool is not engaged in any other shaft for the bedding purpose, the distance between the spool excitation diameter and the spool bearing is reduced to $\approx$ 15 mm. Also, this leads to a decrease in the bending moment around the spool rotation axis. Additionally, the eccentric shaft is removed from the design which means that there is no constraint on the working range of the spool (apart from the slot).

2.7. Design Parameters' Choice

The goal of this section is to determining the design parameters of the assistive device including the pulley diameter (R), spool radius (r_{spool}), maximum elongation of the bungee (Δl), and the ball-screw stroke (S).

As a first step, r_{spool} is calculated as $\approx$ 80 mm through (2.9) by substituting $l_f = 119$ mm, and $\theta_{max} = 85°$. Also, +5 mm tolerance is added to compensate for the small variation of θ_{max} value due to the possible assembly errors. Therefore, 85 mm is determined for r_{spool} (see Table.2.1). In addition, the pulley diameter is assigned as 40 mm (similar to the previous prototype [42]) to calculate the desired bungee force (F_B).

As all the terms are known in (2.7), F_B and F_D are calculated, and the trends of them are presented in Fig.2.12a. After that, ϕ 10 mm endless bungee, shown in Fig.2.3a, is selected

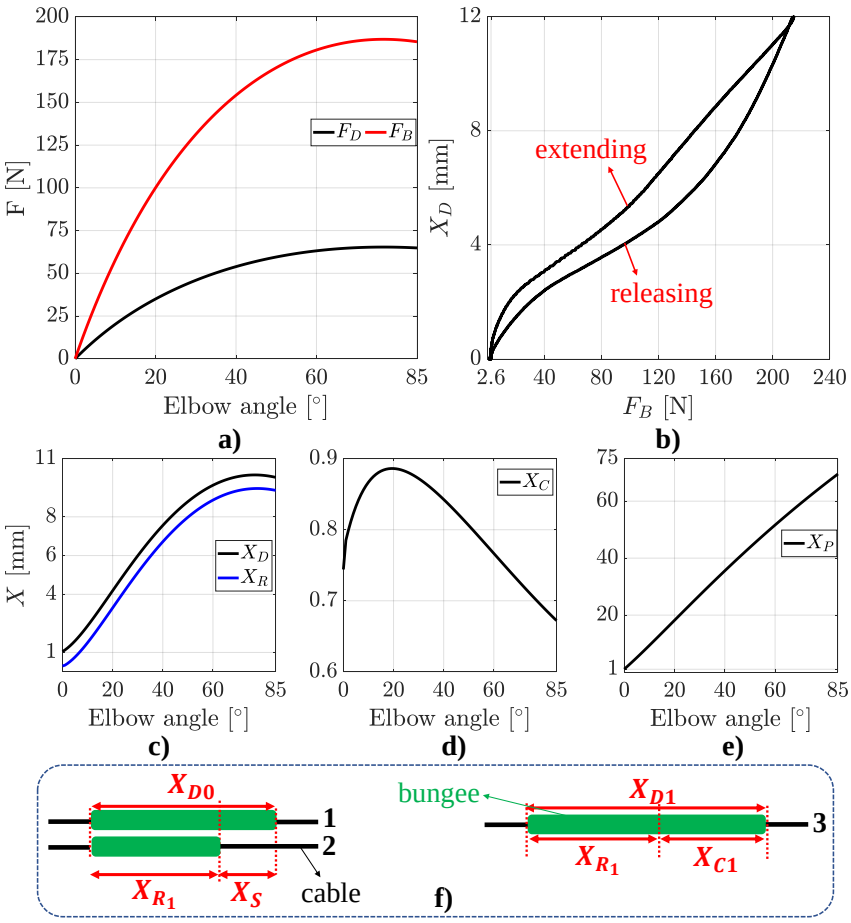

Figure 2.12: a) The desired bungee force (F_B) and the cable force (F_D) graph to balance the W_L, b) Stiffness profile of an endless ring type of bungee (thickness ϕ 10 mm initial length 55 mm), c) Desired (X_D), and remaining (X_R) bungee lengths. d) Compensated bungee length (X_C), and e) The plate position trend. f) Bungee elongation change diagram where 1, 2, and 3 represents the state-1, state-2, and state-3, respectively.

considering its maximum elongation (45% of its initial length) at the corresponding elastic force. It is clear that the selected bungee can generate the desired force under the range of maximum applicable elongation (see Fig.2.12b). Besides, this thickness has the highest stiffness value in the category of endless bungee components.

Table 2.3: Ball-screw stroke computation methodology

$\theta_{elbow}[rad]$	X_D [mm]	X_R [mm]	X_C [mm]	X_P [mm]
θ_0	X_{D0}	X_{R0}	X_{C0}	X_{P0}
θ_1	X_{D1}	X_{R1}	X_{C1}	X_{P1}
$\vdots$	$\vdots$	$\vdots$	$\vdots$	$\vdots$

Regarding the ball-screw stroke, a computation methodology is developed in Matlab®using the selected bungee model (see Fig.2.12b), and all the design parameters that are presented in Table.2.1. To acquire the bungee model, it is directly connected with the load cell excluding the spool system, and tensioned up to 12 mm, and then released back. Then, the resultant curve (only extension state) is fitted to a function presented in (2.11), in which A, B, and C are 0.0002, 0.0114, and 1.0440, respectively. The reason why there is a force reduction in Fig.2.12b when the bungee is released from the extended state is due to its intrinsic damping feature dissipating certain energy from the system. This behaviour is observed in other variable damping joints as well [32].

Considering the bungee model in Fig.2.12b, and the desired bungee force in Fig.2.12a, the former and the latter start from 2.6 N ($F_{B_{Min}}$), and 0 N, respectively. Therefore, it is clear that the experimentally acquired bungee model can be used for the calculation of X_D between 2.6 N, and 215 N. The reason why F_B does not start from 0 in Fig.2.12b is that a bias pretension is set on the bungee ($X_{D0} = 1$ mm), which is $F_{B_{Min}} = 2.6$ N, to remove the backlashes in the experiment structure, and slack on the tendon. Next, the X_D is initialized in the controller, and then the bungee is extended with the applied bias. Thus, the X_D value of this bias is not demonstrated in Fig.2.12b since the reliable bungee data can be used after this pretension. Therefore, an assumption is introduced that if $F_B \leq F_{B_{Min}}$, then $X_D = X_{D0} = 1$. For the F_B values greater than $F_{B_{Min}}$, the obtained bungee model can be employed in (2.11) for the ball-screw stroke computation methodology.

The main goal of the methodology is to acquire theoretically the desired bungee force (see Fig.2.12a) throughout the elbow motion range taking into account the physical conditions (cable slack) at each discrete elbow angle. To explain the method clearly, the formulation is built for two elbow angles. To start with, 5 columns and 2 rows are illustrated in Table.2.3, and the mathematical meaning of those terms are as follows:

$$X_S = R\Delta\theta, \quad X_{D1} = (A)F_B^2 + (B)F_B + (C) \tag{2.11}$$

$$X_{R1} = X_{D0} - X_S, \quad X_{C1} = X_{D1} - X_{R1} \tag{2.12}$$

$$X_{P1} = X_{C1} + X_{P0}. \tag{2.13}$$

According to the developed method, the forearm is almost fully extended ($\theta_0 = 0.001°$)

in the beginning, and all other terms are computed according to θ_0. For instance, the desired pretension on the bungee (X_{D0}) at that angle is the initial pretension ($X_{D0} = 1$ mm in Fig.2.12c). This state-1 is also illustrated in Fig.2.12f with a diagram. When the arm is moved by θ, a certain amount of cable wrapped around the pulley slacks (X_S), and bungee releases (state-2). The parametric calculation of its is reported in (2.11). As the $\Delta\theta$ is considered as 1° in this methodology, and R is constant, X_S is computed as ≈ 0.7 mm for each iteration. Therefore, the remaining bungee elongation (X_{R1}) can be calculated using (2.12). To extend the bungee for the θ_1 (state-3), X_{D1} is calculated, and subtracted from X_{R1} to compensate the new desired bungee elongation (X_{C1}). Finally, X_{C1} is summed with the initial position of the plate (X_{P0}) in (2.13) as the bungee is elongated through the plate. Although it looks like there is a constant shift between X_D, and X_R according to Fig.2.12c, the difference between them is X_C according to (2.12), and it has a nonlinear trend drawn in Fig.2.12d. Also, the X_P profile (see Fig.2.12e) is not exactly linear due to the trend of X_C since X_P is calculated summing X_C terms in (2.13).

Note that the difference between X_{D0}, and X_{R1} is always constant ($X_{R1} = X_{D0} - X_S$), however for the corresponding each iteration (X_{D1}, and X_{R1}), there is a nonlinear difference between them due to the X_D profile. These iterations are continued until θ_{max} is reached. As a result of this computation methodology, the ball-screw stroke is computed as 70 mm (see Fig.2.12e), and 10 mm tolerance is also added to its length. Moreover, the maximum desired bungee elongation is also computed $\approx 20\%$ of its initial length, which is less than the applicable maximum elongation.

2.8. Motor & Ball-screw Selection

After the determination of the design parameters, the motor and the ball-screw selection is carried out taking into account the maximum bungee force, lead and efficiency of the ball-screw. The desired motor torque is computed as follows:

$$\tau_{Motor} = \frac{(F_B)(lead)}{(2\pi\delta)} \tag{2.14}$$

where δ is the efficiency of the ball-screw, and its considered as 0.8 based on the data-sheet. For the desired velocity, the objective is to perform 30 deg/sec at the elbow joint, and on the actuation side, it is expected from the plate to complete the stroke (S) in ≈ 2.83 second (θ_{Max}/V_{Max}) when the elbow is fully flexed/extended. Based on this information, the straightforward ball-screw calculations are carried out considering the lead of the ball-

screw, the stroke, and the desired elbow velocity to acquire the motor velocity (V). The results and motor options are reported in Table.2.4.

Table 2.4: Desired motor torque & velocity values

lead (mm)	V (min^{-1})	τ_{Motor} (Nm)	*MAXON® Motor models*
3†	529.4	0.089	ECXTQ22XL, GPX22UP
4	397	0.119	393879
5	317.6	0.142	426450, GP22

Apart from the velocity and the torque values, the motor weight is also taken into consideration. Hence, the first combination, which is pointed out with †, is selected since it has the lightest weight (206 g) among them. The continuous torque and the velocity values of the selected motor are 0.260 Nm, and 1139 RPM, respectively.

2.9. FEA Simulations of Critical Parts

As the final step of the design methodology, FEA simulations are carried out in Solidworks® performing standard high-quality solid mesh for the most loaded and the critical parts (see Fig.2.13). All the components are simulated under 185 N static force, which is the maximum value of the F_B according to Fig.2.13a. The upper limit of the safe displacement value at the loaded surfaces is identified as 0.05 mm for all the components.

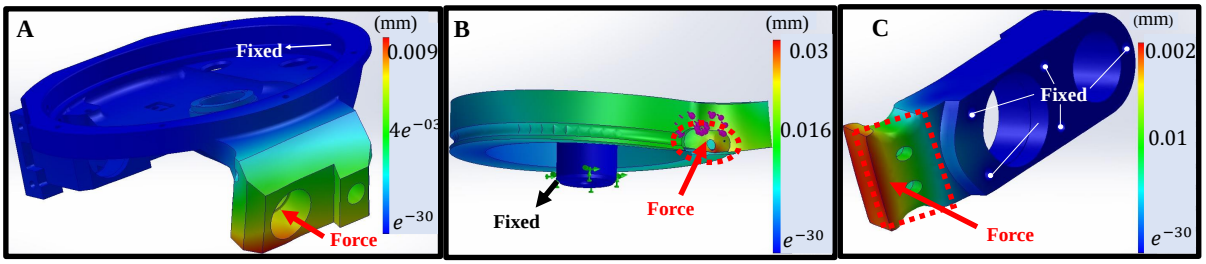

Figure 2.13: FEA simulation results of base (A), pulley (B), and plate (C). The element size/tolerance (mm) of the meshes are 2.628/0.131, 1.853/0.092, and 2.327/0.116 for base, pulley, and plate, respectively. 7050 aluminium is selected for the material of the parts in the simulation, and in the real prototype.

Starting with the base, two bearings are used for each side of the ball screw to compensate for the radial and the axial loads. As expected, the critical loading emerges axially in one direction due to the bungee pretension. Therefore, on a surface, where the outer ring of those bearings has contact, is applied the determined force value to monitor the displacement. Additionally, the hole, where the spool bearing is mounted, is selected as

the fixed surface in the simulation. The resultant maximum displacement is acquired as 0.009 mm. Then, another critical connection surface is detected on the pulley, where the generated elastic force is applied. Also, its shaft is fixed (see Fig.2.13B), and the assigned force value is applied on the critical surface. The displacement is obtained as 0.03 mm.

Finally, the plate is simulated considering its connection surface with the bungee guides. To clarify, first, the bungee is mounted on two guides (illustrated with gray in Fig.2.11), and one of those guides (right side) has a contact surface with the plate. Moreover, a ball screw nut is assembled with four screws on the plate for linear motion. Thus, those connection points are used as the fixed surfaces in the simulation. The same force value is exerted on the bungee guide-plate surface, and the resultant displacement is detected as 0.002 mm. Consequently, it is clear that the acquired displacements on the components are intolerance, which verifies the mechanical design.

2.10. Design of Arm Attachment and Benchtop Setup

In the next step, the design of the arm attachment and the benchtop setup is carried out to evaluate the performance of the developed actuation system, and eventually to build a wearable support device. As can be seen in Fig.2.14, the actuation system is attached to the back of the human, and the generated force is transferred to the right arm. First, the attachments are designed for the back and the arm. For the former one, a compliant back brace is used, and a piece made from hard plastic is assembled on it to attach the actuation system. For the elbow attachment, a compliant elbow brace is used, however, it is modified with respect to the design needs mentioned below.

- It shall allow the human to perform flexion/extension movements throughout the targeted motion range in the sagittal plane.
- It should permit to transfer of the generated force from the actuation system to the arm through the tendon.
- A load cell has to be attached to this brace to measure the tendon force to monitor the generated force in the assistive device.
- An encoder should be coupled with the arm brace to measure the position of the forearm.
- As the forearm performs the relative rotational movement with respect to the upper arm, the direction of the load cell has to be changed depending on the forearm pose (θ).

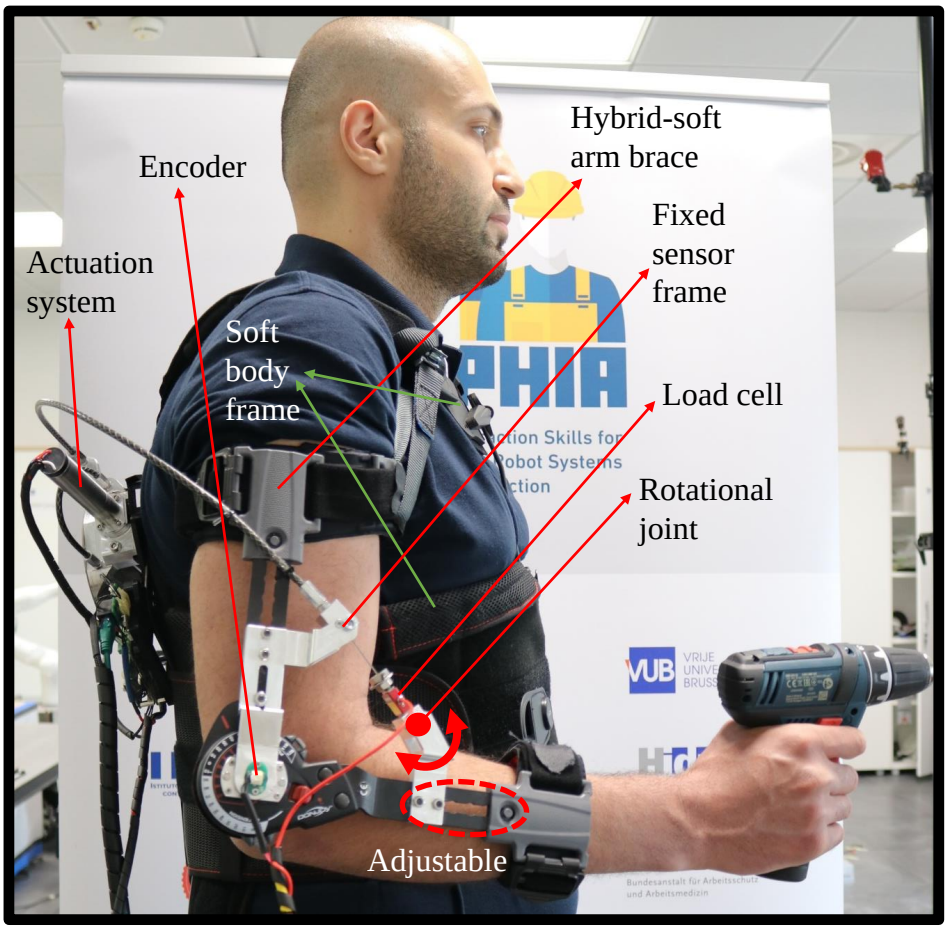

Figure 2.14: The illustration of the developed elbow effort-compensation device on a human subject. An actuation system is placed on a compliant frame together with the fixed sensor frame where the load cell and encoder are attached. A mechanically adjustable compliant arm brace is designed to place it at the center of mass of the forearm for different subjects.

- The arm attachment for the forearm should be mechanically adjustable since its position determines the center of mass of the forearm from the elbow rotation axis ($b + c$ in Fig.1.7), and this distance varies from one person to another.

Focusing on the abovementioned goals, a fixed sensor frame is designed using 7050 AL material and assembled on the compliant arm brace taking into account the previously mentioned fixed attachment distances (a, b) and variable arm distances (c, d) in Table.2.1, and Fig.1.7. A load cell and an encoder are placed on this frame. Moreover, a small rotational joint is designed and coupled on one side with the load cell, and on the other with this frame to allow the load cell to rotate together with the forearm.

Additionally, a benchtop setup is designed considering the similar requirements stated

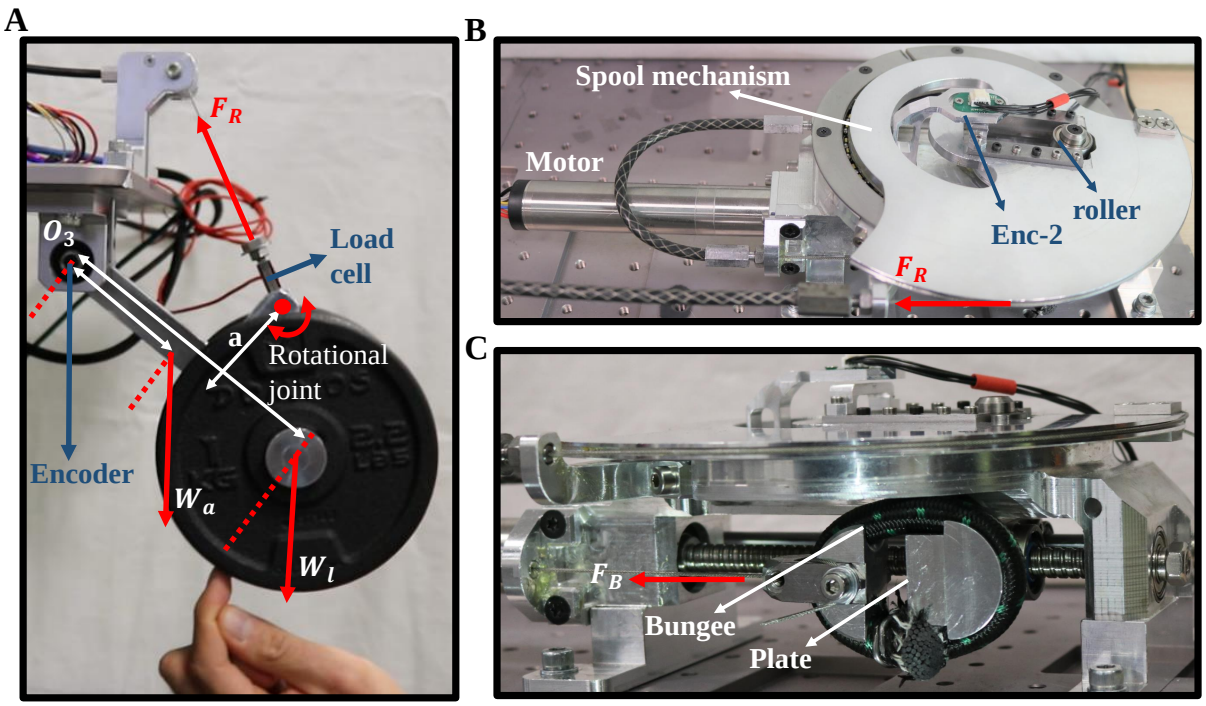

Figure 2.15: The benchtop setup where a load cell, an encoder, and a payload are attached on a rigid link (A), the top view of the manufactured actuation system (B), and the side view of the actuation system in which the bungee is assembled on the plate to regulate its elongation with the help of the ball-screw and the motor (C).

above with the bullet points. The principle motivation of such a setup is to decouple human compliance from the actuation mechanism and to demonstrate the novelty and the performance of the device through comprehensive analysis expressed in Chapter.4. Therefore, similar sensors including the load cell and the encoder are attached on a rigid link (see Fig.2.15A), and a payload is hung to reach the equivalent torque values that of a human with the max payload (1 kg) written in Table.2.1. A rotational joint is used to attach the load cell to achieve adaptation to the link motion as it is done for the arm attachment design. The distance between W_L and O_3 is $l_l = b + c$. Instead, the lever length between the weight of the link (W_a), and O_3 is l_a, which is 127 mm.

2.11. Conclusion

In this chapter, the design of the elbow effort-compensation device is studied starting from the desired max payload at hand to be balanced by the device. Then, the motion range, and the velocity of the elbow, which the exoskeleton is supposed to provide, are determined according to the industrial use cases of the SOPHIA European project. Next, force and

kinematic analysis are carried out to compute the desired torque of the elbow, the tendon force, and length that the assistive device shall supply. Afterward, an endless ring-type of bungee elastic element is incorporated into the actuation mechanism to achieve compliant force transmission between the actuator (i.e., motor and the ball-screw) and the end-effector (i.e., human arm or benchtop). Also, thanks to the intrinsic damping feature of bungee, impact forces or vibrations because of control issues can be absorbed passively similar to human muscles. In the next step, the possible spool mechanism alternatives are investigated in view of some criteria specified to maximize the bungee force transmission while optimizing the energy consumption of the actuator, that is, the size of the motor.

Later on, the 3D-printed prototype is manufactured to verify the functionality of the actuation mechanism under lower forces. Thanks to this prototype, the motion range, and the output force profile of the mechanism are verified by conducting open-end and fixed-end experiments. These tests demonstrated the limitations of the mechanism such as the stretching and bending issue of critical parts, which eventually prevents to increase in the output force of the device. The motion range of the elbow is also limited due to this preliminary design.

To tackle with those challenges, an optimization is carried out in the mechanical design, and then a computation methodology is studied to select the design parameters. Afterward, FEA simulations are conducted to monitor the displacements on the critical parts under the computed maximum bungee force. Finally, the arm attachments and the benchtop setup are designed considering a number of criteria, and the targeted design performance values such as a, b, c, d parameters in Table.2.1. The manufactured prototype of the actuation mechanism is illustrated in Fig.2.15 (B and C). In the next chapter, several control strategies are presented to be employed on the developed assistive device.

3 | Control of the Elbow Effort-Compensation Device

The goal of this section is to express the control techniques developed to be implemented on the elbow effort-compensation device. Those methods are divided into two to be the classical and the adaptive control approaches. The fundamental focus is to achieve load compensation and load release tasks to reduce the effort on the wearers' biceps muscle, which is the primary muscle for balancing a load at hand when the upper arm is in a vertical position with respect to ground.

To begin with, the classical controller covers only PID (Proportional-Integral-Derivative) type controllers, where all the input parameters are set manually (e.g., elbow position or desired force profile on the tendon), and the output is determined based on the design of the actuation mechanism (e.g., bungee elongation). Therefore, the aforementioned controllers are formulated to demonstrate if the assistive device is met with the design requirements such as motion range, velocity and the torque reported in Table.2.1. Also, sensitivity analysis is performed to generate force references for multi-subject by setting different forearm weights (W_a) and arm distances (c, d) in (2.2). As mentioned in the previous chapter, the force references are calculated for the forearm and the external load compensation.

In addition to the classical controller, adaptive control strategies are employed through complex algorithms to accomplish extensive tasks. To clarify, the load compensation is performed by estimating the load at hand with the help of an EMG (Electromyography) sensor attached to the biceps, and eventually generating the new force reference automatically thanks to the developed algorithm. Afterward, when the load is released from the hand, the device cannot detect this load change and continues to support the user for the previously estimated payload. Thereby, excessive assistive forces are transferred to the wearer, causing an unsafe operation. The solution is proposed by constantly monitoring the power of the exoskeleton, which is calculated taking into account the tendon force and the velocity. Then, a power threshold is identified considering the users' periodic motions

under the maximum payload. At the instant when the arm suddenly accelerates in an upward direction due to the load change, the power increases sharply, and this triggers the load release algorithm to exclude the force reference for the external load. Therefore, the user can continue to perform an operation with the only forearm compensation.

The targeted performance metrics to fulfil in the control of assistive device are stated as follows:

- high performance force tracking for user transparency, and effort reduction,
- fast and smooth load compensation and load release,
- repeatability of the above-stated operations on multi-subject,
- intrinsic adaptation to sudden reflexive movements or impacts.

3.1. Classical Control Methods

The classical control methods are also investigated under two subtitles as force and the position control. Both of the techniques are employed for only load compensation tasks.

3.1.1. Force Control

Primarily, force control is adopted in the assistive device to generate the force references as a function of the design parameters in Table.2.1. The controller is divided into two stages as the high-level controller (HLC), and the low-level controller (LLC). The load compensation action is included in the HLC presented in Fig.3.1. Then, the force references to achieve that task are generated and fed to the PID regulator. Thus, as a first step, the derivation of input force reference (F_R) is explained through (2.3). To clarify, L, and α are constant parameters that are calculated taking into account the fixed sensor frame dimensions (a, b in Fig.2.2). Next, there is τ term, which includes θ, the forearm weight (W_a), the external load (W_L), and the lever lengths (l_a, and l_l). Apart from θ, all of them are assigned in the beginning of the operation (c, d, W_a, W_L).

During the task, as the user moves his/her forearm, the force reference is generated as a function of the elbow position. This way of working includes the human intention in the control loop since the input command comes from the wearer. Thus, the flexibility of human increases in the targeted task, and we call this strategy as 'human-in-command control'.

Therefore, in the next step, the sensitivity analysis is conducted to calculate the input force

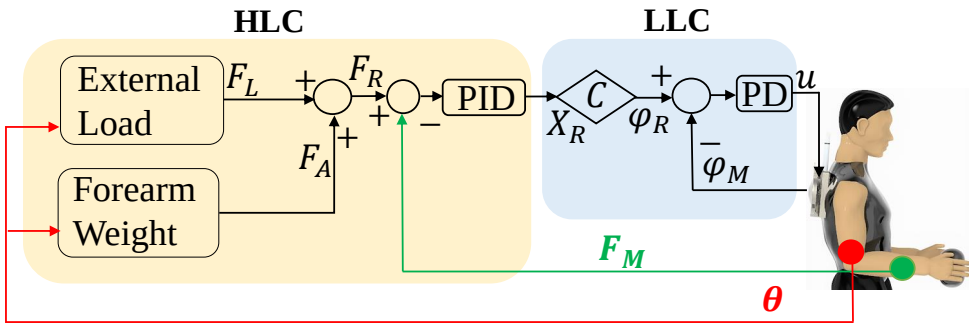

Figure 3.1: The developed force controller diagram for load compensation. HLC and LLC represents high-level and low-level controller.

profiles for different users' forearm/body specifications (c, d, W_a) as in [4]. In Table.3.1, the c, d, W_a data of 6 subjects are presented (Note that "S" refers to subject). Also, several experiments are conducted on these subjects expressed in chapter-4.

Table 3.1: The forearm specifications of the subjects.

Subjects	c [mm]	d [mm]	W_a [N]
S_1	70	170	20
S_2	30	130	15
S_3	50	150	20
S_4	50	150	15
S_5	50	150	20
S_6	50	150	20

To begin with, the average value of anthropomorphic c/d values are 50/150 mm based on [14],[6], which means the center of mass of the forearm is measured as the middle point in between the elbow center of rotation and the hand. Considering this information, a similar strategy is used to measure participants' arm dimensions, and results show that majority of them (S_3, S_5, S_6) comply with the average c, d anthropomorphic values, however, there are small changes for other subjects reported in Table.3.1. Therefore, c values are adjusted mechanically for the participants on the elbow brace (see Fig.2.14). When it comes to W_a values, it is set 20 N for male subjects according to [6]. For the female subjects, 15 N W_a is set, and the details of this selection is explained in chapter-4.

Next, the summation of F_L, and F_A in (2.3) is the total force reference (F_R) to compensate the external (W_L) and the internal loads (W_a). As mentioned earlier, W_L is set as 1 kg (max allowable external load value of the device) in (2.3) in the calculation of F_L. While S_1, S_2, and S_4 have different forearm specifications, S_3, S_5, and S_6 have the same data. Therefore, the F_R profiles are computed for S_1, S_2, S_3, S_4, and presented in Fig.3.2.

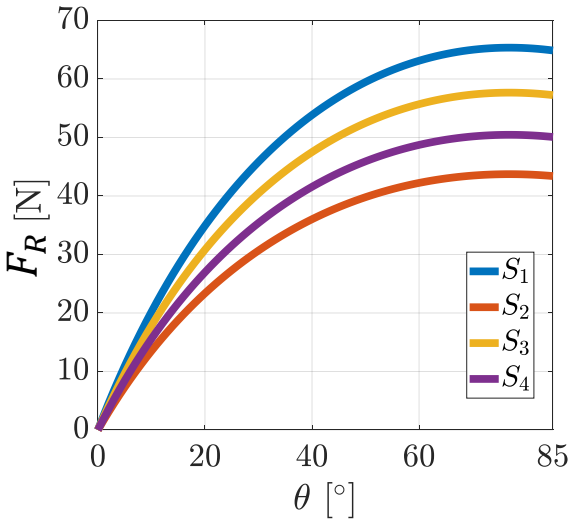

Figure 3.2: Sensitivity analysis of the assistive force (F_R) for different arm dimensions (c, d) and forearm weights (W_a).

After acquiring the input of the PID regulator in HLC (i.e., input force references), the output is calculated as the desired plate position (X_R) due to the series elastic actuation design approach. To control the plate position, a PD controller is implemented in the motor, and this stage is identified as LLC. In this controller, the desired plate position is always considered as the reference, and then the corresponding motor position reference (φ_R) is calculated taking into account the transmission from plate to motor (motor gear ratio and the ball-screw). Then, the actual motor position (φ_M) is also measured, and hence the input and output of the controller is the motor position error, and the controlled motor position, respectively.

To compute the minimum position change of the plate (X_{min}), the position resolution of the motor, which is 15° based on the datasheet, is considered. Then, the gear ratio (GR) of the motor (3.9:1), and the ball-screw lead (3 mm), are taken into account, and X_{min} is calculated as $\approx$ 0.2 mm using (3.1). This resolution is accepted under tolerance for the targeted application because 0.2 mm plate error generates $\approx$ 5 N force error at the bungee side based on the average value of bungee stiffness ($\approx$ 27 N/mm). The effect of this error on the tendon (F_d) is $\approx$ 2.3 N according to (2.5).

$$X_{min} = (lead)\frac{(\theta_{Motor})}{GR}. \tag{3.1}$$

3.1.2. Position Control

Another way to perform load compensation with the help of the developed assistive device is the position control through the attached encoder on the elbow. In this case, the input of the PID regulator in HLC is the position error, calculated by subtracting the measured elbow position (θ) from the desired (θ_d), while the output is again the desired plate position. Finally, the desired plate position is tracked by the plate controller as mentioned earlier. In such a control scenario, human intention is excluded from the control loop since the device follows the predefined desired position trajectory.

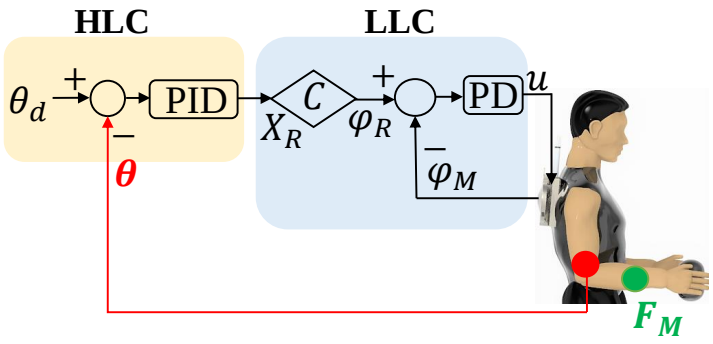

Figure 3.3: The developed position controller diagram for load compensation. HLC and LLC represents high-level and low-level controller.

Additionally, thanks to the elastic element, the device can be operated in a semi-active way. The bungee can be elongated at a distance to balance the arm at a position, and then aggressive movements such as an impact can be performed. This mode of operation requires to perform only LLC, controlling the desired plate position with the help of PD regulator.

3.2. Adaptive Control Methods

Adaptive control techniques are studied in two steps defined as load compensation and load release. Force control is performed in both of the actions, yet the load changes at hand are detected automatically owing to the developed algorithms, and additional sensors.

3.2.1. Load Compensation

The main purpose of the load compensation algorithm is to estimate the load at hand when the user holds it. First, an EMG is attached to the biceps, and only the forearm is

supported (F_A) by the device. No load is held during this process at hand, and the user is asked to conduct cyclic movements. Next, the peak values of the measured EMG data are detected, and the root mean square of those peaks are computed. The resultant value is assigned as the minimum effort level (T_E) for each subject.

Table 3.2: Load estimation algorithm parameters

a, b, c, d [mm]	W_{Max} [N]	θ_C [°]	t_i, t_t [s]
$50, 100, 50, 200$	10	$50 \leq$	$0.001, 1$

After T_E is identified, any external load introduced to the system (user holds an object in the hand), will result in an increase in the EMG signal. Thereby, the load estimation is initiated generating F_L as a ramp function on the tendon to assist the user. For the derivation of the slope of this ramp function, first, maximum value of F_L in (2.3) is computed considering the load estimation parameters. To begin with, θ_C (applicable elbow angle) is identified as minimum 50° ($\theta_{C_{MIN}}$) or above for the load estimation since the EMG values change depending on the arm configuration. As expected, it is very low when the arm is at fully extended position, which means $\theta = 0$ in (2.1), and the effort (τ) in elbow joint is close to zero (This prevents conducting load estimation).

After the parameter determination, $F_{L_{MAX}}$ is computed as $\approx$ 30 N through (2.3) by substituting $W_L = W_{Max} = 10$ N, $\theta = \theta_{C_{MIN}}$, and other parameters (i.e. l_L, L, and γ using a, b, c, d in Table.3.2). We targeted to generate $F_{L_{MAX}}$ in 1 second for proof-of-concept. As the controller update rate is 1 kHz, F_{inc} (slope of the ramp function) can be computed as follows:

$$F_L = F_{L_P} + \overbrace{F_{L_{MAX}} \frac{t_i}{t_t}}^{F_{inc}}, \quad W_L = \frac{F_L L \cos(\gamma)}{\sin(\theta) l_L} \tag{3.2}$$

where t_i, t_t, and F_{L_P} represents the controller update rate, targeted load estimation time, and the previous value of F_L, respectively. F_{inc} can be calculated as 0.03 N in (3.2). Next, W_L is isolated from (2.3), and written in (3.2). F_L is increased (starting from 0) adding F_{inc} on the F_{L_P} to compute the estimated load in this equation.

During this interval, when the EMG reduces below T_E, the force increment (i.e. F_{inc}) is terminated, and the load is estimated. Therefore, F_L is updated according to the estimated load throughout the elbow motion range in (2.3), and the EMG signal is eliminated from the controller. Noteworthy, in recent works, the EMG is used for assistance in which

its value is multiplied with a gain that has to be regulated during the operation by the wearer [35], or a fixed gain [47] potentially increasing the mental load of the wearer. Instead, our approach does not require EMG signal during the task as the load is estimated only once through the arm attachment geometry, and the position of the elbow. Additionally, since the main design idea of the device is to reduce the effort for repetitive tasks, the success rate for load estimation is assumed as a minimum 70% of the actual load. As the upper limit of the load estimation, +1.5 N is added to the actual load to avoid excessive support on the arm (e.g., if the actual load is 10 N at hand, the estimation of W_L is acceptable up to 11.5 N).

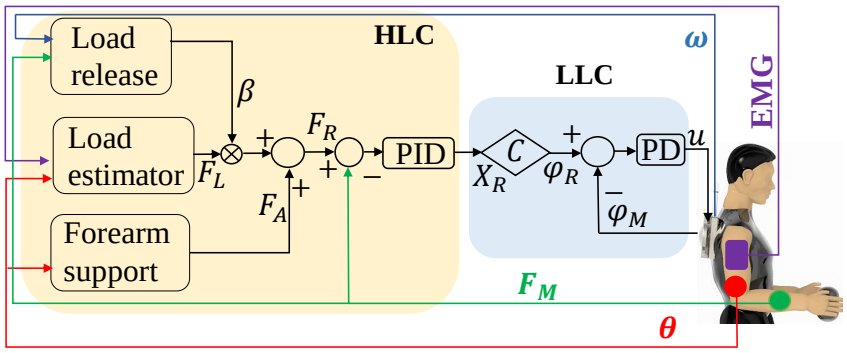

Figure 3.4: The developed adaptive controller diagram for load compensation and load release tasks. HLC and LLC represents high-level and low-level controller.

3.2.2. Power-Aware Load Releasing

As previously mentioned, one of the challenges of assisting people using wearable devices with force control is to adapt the exoskeletons' response when the object, held by the user, is released from the hand. At that instant, the device pushes the arm in an upward direction since the force reference is generated for the load and the forearm.

To achieve a fast force reference transition to only forearm support, yet smooth and intuitive, we correlate the output power and the force reference of the exoskeleton. Starting from the former one, it is supplied through a tendon cable (wrapped around the spool) to the user. Therefore, the calculation of the power (P_{Exo}) is conducted based on the velocity ($\dot{x}$) and the force (F_M) of the tendon in (3.3).

$$P_{Exo} = F_M \dot{x}, \quad \dot{x} = r_{spool}\omega \tag{3.3}$$

In the method, first, a power threshold (P_{Max}) is set taking into account the max payload (W_{Max}) and the elbow velocity that the exoskeleton shall generate to assist the user for a

task. Next, when contact is lost between the object and the user, the P_{Exo} goes beyond the P_{Max} due to a sudden load change. Accordingly, the force reference for the load (F_L) is multiplied by the coefficient β (see Fig.3.4), which becomes zero to eliminate the portion of F_L in (3.4). Hence, only arm support (F_A) is fed to the system as the force reference to achieve an adaptation to the load change.

$$F_R = F_L\beta + F_A \tag{3.4}$$

$$\beta = \begin{cases} 0, & \text{if } P_{Exo} > P_{Max} \\ 1, & \text{otherwise.} \end{cases} \tag{3.5}$$

Consequently, the proposed method allows the wearer to perform motions with W_{Max} unless the P_{Max} is exceeded. Moreover, the reason for the unidirectional power threshold is that the unsafe movement (pushing in an upward direction) can only take place in flexion movement since the effort-compensation device stores the energy in this direction by tensioning the bungee. For assistance in extension, this stored elastic energy is used by releasing the bungee depending on the arm position. Since the sign of the power in flexion movement is positive due to the direction of F_M and $\dot{x}$, the P_{Max} is assigned as a positive value expressed in the next chapter.

3.3. Conclusion

In this unit, control strategies are explained to carry out load compensation and load release tasks on the developed elbow effort-compensation device. The algorithms are categorized into two steps to be classical and adaptive control. The former one includes only a simple PID regulator whose input is elbow position, plate position or desired force to conduct load compensation action. The parameters of those input signals (e.g., W_L for force control) are identified manually, while the output is the plate position to regulate the bungee elongation with the help of the motor. The sensitivity analysis is also implemented to compute force references for subjects with different forearm specifications.

Later on, the above-mentioned control approach is extended, and adaptive strategies are developed to achieve more complex tasks. To start with, the load compensation is accomplished with the help of the EMG-based control interface, generating the force reference automatically for the estimated payload at hand. Next, a power-aware load releasing control technique is proposed to perform adaptation to the load change. For

instance, the challenge is detected in the literature that according to our knowledge, there is no any work to tackle with the load release action when the exoskeleton is controlled under force. What happens at that instant is that the device cannot recognize the fact that the load is released by the wearer. Thus, extreme assistive forces are transferred to the user. To overcome this issue, a load releasing control method is designed by continuously tracking the power of the device. When the power surpasses the predefined limit calculated taking into account the periodic movements of the wearer under the maximum payload, the external load portion of the force reference is removed from the control equation. Hence, the human can perform the task under only forearm compensation safely. In the next chapter, the validation of the presented control algorithms are expressed by conducting several comprehensive analysis and experiments.

4 | Experiments and Results

The goal of this section is to demonstrate the effectiveness, and performance of the developed effort-compensation device through several experiments. The designed test protocols are classified into two subtitles to be the design, and adaptive control validation tests. The former, and the latter are carried out by making use of the previously explained classical, and adaptive control techniques, respectively. The tests are conducted on both benchtop in Fig.2.15A and human subjects in Fig.1.7.

4.1. Design Validation Experiments

In this chapter, the experiments are structured to focus on the strength of the design through simple control algorithms. For instance, a number of analyses are carried out to demonstrate the impact and vibration isolation capacity of the bungee, energy analysis, force tracking performance, and effort reduction percentages. First, only the actuation system verification tests are carried out on a benchtop setup. Next, human experiments are conducted.

4.1.1. Actuation System Verification

The actuation system is tested on a rigid link, which is manufactured with the same dimensions as the arm attachments distances, presented in Fig.2.15A. Also, different payloads are hung on this link to see if the design can meet the targeted values reported in Table.2.1. In the experiment setup, a load cell (FUTEK-LSB201) is attached to the link to measure the cable tension, and a 2 Hz Butterworth low-pass filter is used to filter the force data. Additionally, two encoders are used to measure the position of the link (Enc-1), and the spool (Enc-2), respectively. 6 Hz Butterworth low-pass filter is applied to both of them. A motor driver and a data acquisition card, which are communicating with the help of EtherCAT at 1 kHz, are utilized to control the system in MATLAB®/Simulink Real-Time interface.

The system can operate under force and position controllers. The reference of the force

Table 4.1: Control gains of the actuation system verification test.

Controller	K_P	K_I	K_D
Force	0.1	6	0.002
Plate	12000	0	5
Position	10	200	0.8

is estimated using (2.3), and it is changed for each payload manually. F_L is generated for $1, 2, 3$, and 4 kg payloads (W_L) for $l_L = b + c$, while F_A is calculated considering the link mass (0.42 kg), and its distance from link rotation axis ($l_a = 127$ mm). Next, the measured force is acquired through the attached load cell, and Enc-1 is used to update the force reference depending on the link angle in (2.2). PID-based force and position controllers presented in section-3.1 are employed with assigned gains illustrated in Table.4.1. Since the system is nonlinear, the control gains are tuned manually.

Experimental Procedure

Four experiments are carried out to evaluate the proposed actuation system. In experiment-1, the force tracking performance during joint flexion and extension movements is verified. A simulation is created in MATLAB®to give visual feedback to the human operator with the help of an avatar to perform the desired movements with 15 deg/sec. During these flexion/extension movements, the actuation system is expected to balance a range (1-4 kg) of payloads.

In experiment-2, a power analysis is carried out while measuring the output (P_O) and input power (P_I) of the system. With the link load of 4 kg, the device is fed with a sinusoidal wave link position reference with 0.055 Hz ($10°/s$), 0.111 Hz ($20°/s$), and 0.166 Hz ($30°/s$) frequencies with 2 repetitions under position control without any external intervention to avoid transferring power to the system. The former is acquired by multiplying the measured force and the cable velocity, whereas the latter is carried out by multiplying the current of the control board and the motor voltage. The cable velocity is computed by multiplying the spool radius with the spool velocity measured through Enc-2. Note that the current sensor is connected between the power supply and the control board to include all the elements' current consumption including the motor.

In experiment-3, the same experimental protocol as experiment-2 is carried out, while the test is conducted with and without the bungee. For both test setup, the same control gains are used to compare the two setups under similar conditions. The motivation of this experiment is to monitor the measured force trends and to prove how the system

intrinsically isolates the vibrations under high frequency movements thanks to the elastic element.

Finally, in experiment-4, the impact isolation capacity of the system is estimated through a ball-catching task. A 1 kg rigid ball is released from 80 mm height to a bowl-shaped plastic part that is assembled with the link (see Fig.4.4c). This test is also conducted with and without bungee setups, and repeated 3 times for both cases to experimentally demonstrate the impact absorption of the bungee. To do that, the plate is moved to a position in which the link position is 90°. Note that only the plate controller is activated, and no control is employed on the link position to allow the link to perform oscillated movements under the impact force.

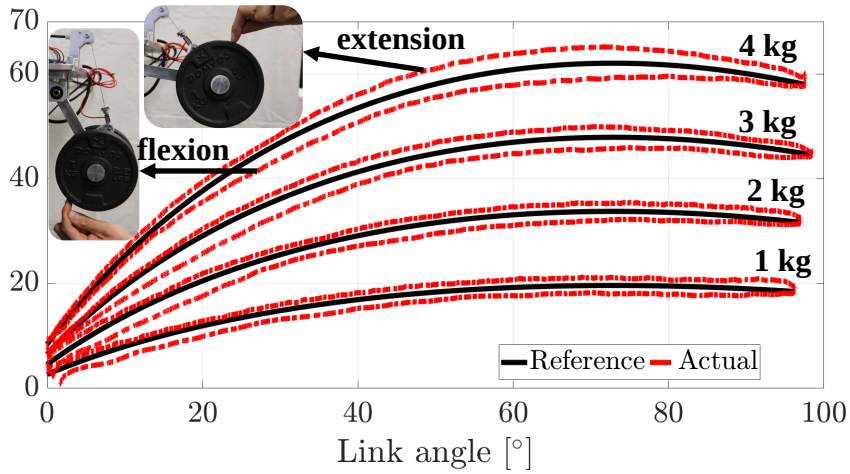

Figure 4.1: Experiment-1 results for balancing different payloads on the link. RMS values of force/plate positions error for 1 kg, 2 kg, 3 kg and 4 kg are 1.38 N/0.23 mm, 1.6 N/0.26 mm, 1.63 N/0.27 mm, and 2.07 N/ 0.33 mm, respectively.

Experimental Results

Based on the experiment-1 results presented in Fig.4.1, the RMS values of force/plate positions error for 1 kg, 2 kg, 3 kg and 4 kg are 1.38 N/0.23 mm, 1.6 N/0.26 mm, 1.63 N/0.27 mm, and 2.07 N/ 0.33 mm, respectively. The plate position error is due to the resolution of the motor that is mentioned before (X_{min}). It is clear that the cable force reaches up to 60 N, and the motion range is measured between 0° to 95°, which meets with design requirements in Table.2.1. The reason why the measured force is smaller for the flexion than the extension movement is that the human operator is applying force to move the hung load for the flexion, and helping the actuation system for the balancing. Instead, for the extension, the user is pushing the elbow, and the measured force becomes greater than the reference. Therefore, those force differences emerge due to the interaction

force, and the force tracking error of the controller.

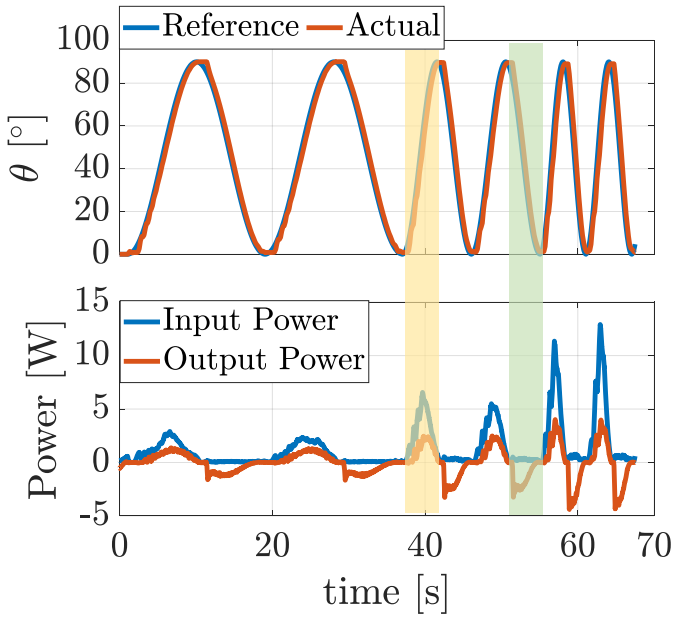

Figure 4.2: The results of experiment-2. Yellow, and green areas on the graph shows the flexion, and extension interval of the link, respectively.

Considering the experiment-2 results in Fig.4.2, as expected, the P_I is always greater than P_O, and their values increase as the frequency of the movement raises. When the link is in flexion interval (highlighted in yellow), P_O is positive while it is negative for the extension (highlighted in green) due to the velocity direction change. The reason why P_I is sharply higher during the flexion than the extension is that the bungee is tensioned until the link reaches its maximum position ($\theta \approxeq 90°$). Then, when the link starts the extension movement, the motor always brakes by releasing the bungee and using the elastic energy that the system stored during the flexion phase. Then, the RMS values of input/output power throughout the experiment are computed as 2.41/1.31 Watt, and the power efficiency is calculated 54.31%. The reason for the power loss is because of the frictions in the system such as tendon connections, the damping effect of the bungee that dissipates some energy from the system, and a small amount of loss comes from the efficiency of the motor and ball screw which are 87%, and 80%, respectively.

In experiment-3 results depicted in Fig.4.3A, the measured force values are demonstrated under repetitive movements at different frequencies with and without bungee cases. To monitor the oscillations in the frequency spectrum, FFT analysis is performed in MATLAB®. As presented in Fig.4.3C, the highest amplitude is observed close to zero frequency since the highest movement frequency of the link is 0.16 Hz. However, after $\approx$ 1.5 Hz, there is a significant magnitude difference in between with and without bungee data, which is

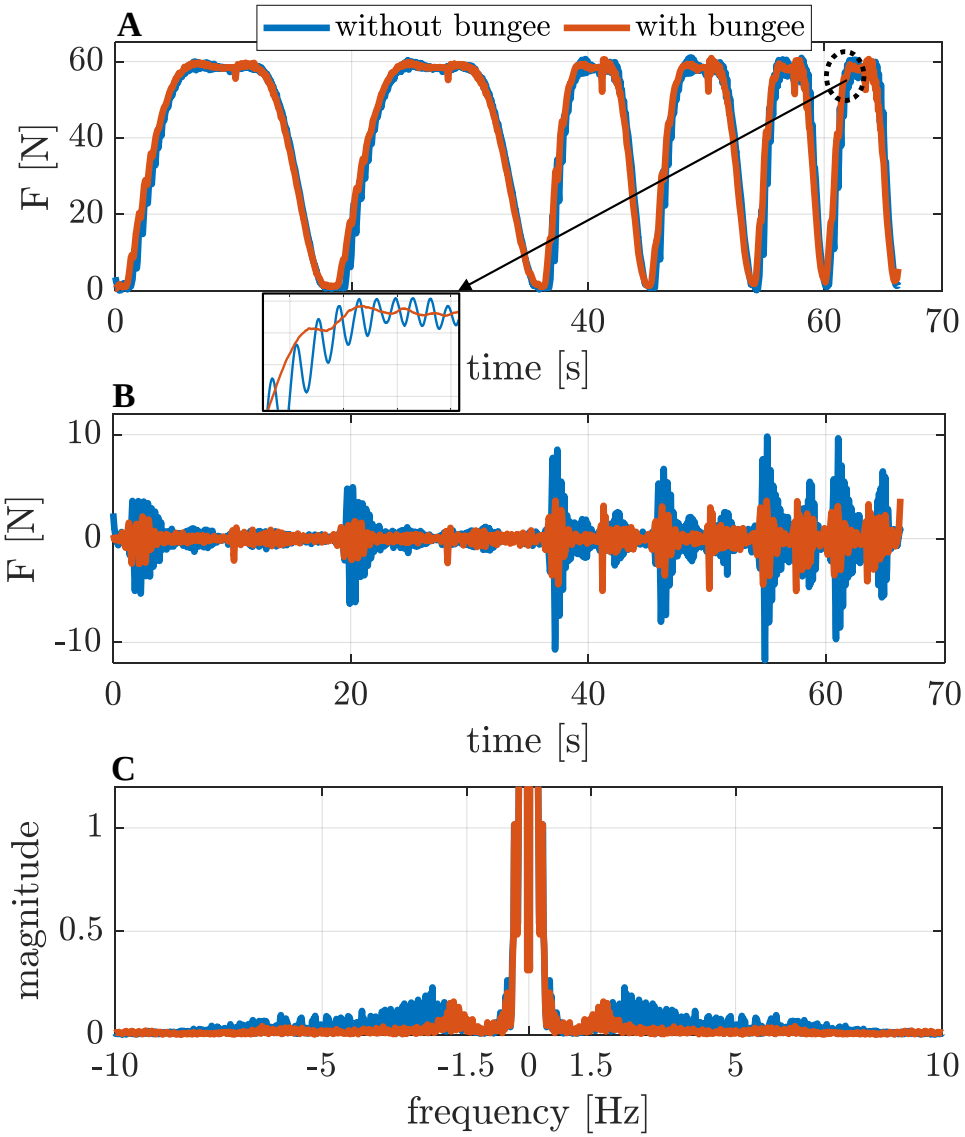

Figure 4.3: The results of the experiment-3 for with and without bungee cases. A) The measured force, and B) its 1.5Hz high-pass filtered profiles. C) The FFT analysis of the measured forces.

due to the vibrations that occur on the tendon (see zoomed view in Fig.4.3). To compute the amount of these vibrations, 1.5 Hz high-pass filter is applied on the force values, and the resultant profiles are illustrated in Fig.4.3B. Taking the RMS values of the with and without bungee data, the vibration reduction is calculated as 50.74% with respect to without bungee case, which is a quite promising result to show the intrinsic vibration isolation ability of the bungee element.

Finally, the experiment-4 results are presented in Fig.4.4 with (a) and without bungee (b) cases. It is clear that the first impact force is slightly higher for without elastic element

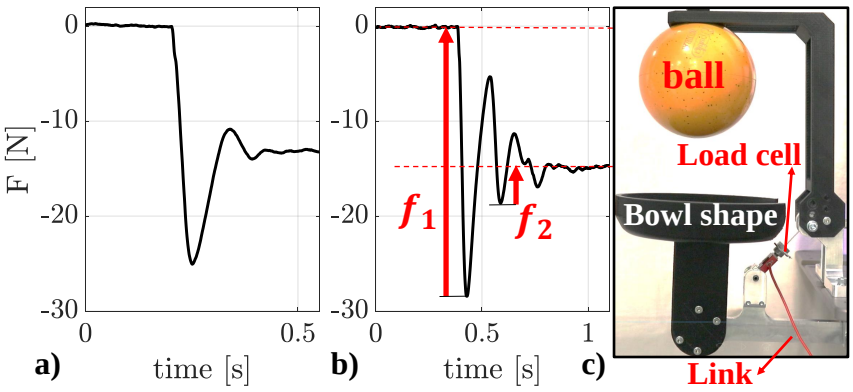

Figure 4.4: Experiment-4 results for with (a), and without (b) bungee cases. The illustration of the experiment setup (c). f_1, and f_2 are the first and second peaks of the impact forces.

than the other. Moreover, the ball only bounces one time for the with bungee setup, and then it is damped quickly. However, for without bungee case, the ball bounces three times with higher impact forces. To estimate the damping ratio for the two setups, the logarithmic decrement is used for the first two consecutive force peaks, and the following formulas are adapted based on [2].

$$\delta = \log\left(\frac{f_1}{f_2}\right), \qquad DRI = \frac{\delta}{\sqrt{\delta^2 + (2\pi)^2}} \tag{4.1}$$

According to the RMS value of 3 repetitive test results, the damping ratio index (DRI) is estimated for with/without bungee as 0.47/0.3. Finally, the percentage of the DRI increment with respect to the without bungee case is calculated as 56.14%, which demonstrates the significant shock absorbing ability of the bungee.

4.1.2. Human Experiments

The developed assistive device is tested on 6 young healthy human subjects (28 ± 3 years old, 2 female, and 4 male) in an equivalent industrial painting task (see Fig.1.7) to monitor the effort reduction, which was carried out at the Human-Robot Interfaces and Interaction (HRII) Lab, Istituto Italiano di Tecnologia (IIT), and approved by the ethics committee Azienda Sanitaria Locale (ASL) Genovese N.3 (Protocol IIT HRII SOPHIA 554/2020).

The heights (subject) of the subjects are 194 cm (S_1), 170 cm (S_2), 179 cm (S_3), 173 cm (S_4), 183 cm (S_5), 182 cm (S_6). A PID-based force control ($K_{PH} = 0.07, K_{IH} = 4, K_{DH} = 0.002$) is employed on the assistive device using the load cell and Enc-1 to include the

users' intention. The method on the generation of the force references for the subjects is explained in section-3.1.1. However, the validation of W_a values assigned for the subjects has not expressed yet. To clarify, it is reported in section-3.1.1 that W_a is set 20 N for male subjects based on [6]. To verify this value, an EMG is attached to the biceps muscle to monitor the effort level under forearm compensation. To do that, only F_A is generated using (2.3), and subjects are asked to do quasi-static motions while measuring their effort. According to the results, their normalized EMG values are less than 2% (considered as lowest EMG threshold), hence, the assigned W_a is accepted for the male subjects.

For the female subjects, 20 N W_a is monitored as excessive support based on their feedback, and this value is reduced to 15 N while measuring their biceps effort level. Similarly, their EMG values are measured below 2%, and 15 N is set for the female participants. As mentioned before, 20 N is the average value for the forearm weight in the literature, but small changes can be expected in between genders. Therefore, the assigned W_a values are also experimentally verified to monitor if the wearers' are supported in a comfortable way.

Throughout the experiments, the muscular activities of the biceps brachii, which is the main muscle for the flexion movement, are recorded through the wireless sEMG system of Delsys Trigno platform by Delsys Inc (Natick, MA, United States). The raw data of EMG is acquired at 2 kHz, and post-processed in MATLAB®using a second order high-pass filter with 0.1 Hz. Then, full-wave rectification is implemented, and finally, a second-order low pass filter is applied with 2.5 Hz.

Experimental Procedure

The designed experimental setting is shown in Fig.1.7, in which a paint sprayer is held by the S_1 and moved across virtual points to represent a rectangular painting path starting from point-1 to 4 in the sagittal plane during 5 minutes. Moreover, participants are prompted to perform movement in the range of $30° \pm 5°$ (lower limit) to $80° \pm 5°$ (upper limit) flexion/extension movement in between points $2-3$ and $4-1$ in $t_1 = 2.5 \pm 0.5$ second. Also, t_2 is defined 1.5 ± 0.5 second for the shifting movement in between point-1 and 2 and point-3 and 4. The participants are guided through an external counter, which gives an audio feedback by counting in between points to finish the task in t_1 and t_2 seconds. Another audio feedback is created to inform the subjects about lower and upper limits of the motion range. If the users' movement is below 25° or above 85°, this is considered the free motion, which is a possible scenario for the workers in the manufacturing lines.

The experiment is conducted with (W/) and without (W/O) assistance case in a ran-

domized order as in [52]. For the latter one, the device is again worn by the user, yet the cables are slack. The EMG, elbow position, and velocity are recorded to compare them 'with assistance' results. 10 minutes rest is also given to subjects in between W/ and W/O assistance tests to avoid fatigue in their muscles.

Experimental Results

The results of the experiment for W/ and W/O assistance cases are presented in Table.4.2, which reports the RMS values of the elbow velocity, flexion/extension time (t_1), force error on the tendon, normalized EMG values, maximum (θ_{Max}), and minimum positions (θ_{Min}), and finally effort reduction percentages for male (M) and female (F) subjects. First, the θ_{Max} and θ_{Min} are detected for each cycle (flexion/extension) on the data, and their RMS values are calculated to compare it with the experiment requirements. Moreover, t_1 values are also computed by dividing the $\theta_{difference}$ ($\theta_{Max} - \theta_{Min}$) to the measured velocity. Results show that apart from the θ_{Max} of S_5 for with assistance case, and θ_{Max} of S_2 for without assistance, all subjects successfully completed the task in the range of assigned velocity and motion range. Moreover, the effort reduction for S_6 is marginally below 50%, showing slightly different results than others. However, the differences between the results and targeted ranges are quite small, and we believe that they can be improved with the short training phase.

Table 4.2: Human Experiment Results

M: Male, F: Female	**Subject-1 (M)**		**Subject-2 (F)**		**Subject-3 (M)**		**Subject-4 (F)**		**Subject-5 (M)**		**Subject-6 (M)**	
c, d [mm], W_a [N]	70, 170, 20		30, 130, 15		50, 150, 20		50, 150, 15		50, 150, 20		50, 150, 20	
	W/	**W/O**	**W/**	**W/O**	**W/**	**W/O**	**W/**	**W/O**	**W/**	**W/O**	**W/**	**W/O**
Velocity $[°/s]$	31.61	33.8	17.94	23.64	22.48	33.83	21.79	30.01	17.78	31.14	22.68	25.86
Maximum Position [°]	78.59	82.84	88.3	71.62	78.47	77.65	75.68	77.76	74.57	77.31	77.42	83.43
Minimum Position [°]	5.45	0.67	37.45	14.43	20.91	1.75	25.32	12.02	29.76	7.82	23.55	3.82
Force Error [N]	5.39	-	4.67	-	4.89	-	5.52	-	4.21	-	4.63	-
$t_1[s]$	2.31	2.43	2.83	2.41	2.56	2.24	2.31	2.19	2.52	2.23	2.37	3.07
EMG [%]	6.24	14.98	10.43	35.75	4.59	18.85	13.36	44.23	5.28	16.17	14.06	25.39
Effort Reduction [%]	**58.34**		**70.82**		**75.64**		**69.79**		**67.34**		**44.62**	

4.2. Adaptive Control Validation Experiments

In this section, the performance of the presented adaptive control interface in section-3.2 is studied through two experimental studies. The first experimental study focuses solely on the validation of the power-aware load release on a bench-top setup (see Fig.2.15A), whereas the second one validates the load estimation method and the power-aware load release on 8 healthy right-handed human subjects (28±3 years old), which was carried out at the Human-Robot Interfaces and Physical Interaction (HRII) Lab, Istituto Italiano di Tecnologia (IIT), and approved by the ethics committee Azienda Sanitaria Locale (ASL) Genovese N.3 (Protocol IIT HRII SOPHIA 554/2020).

In the benchtop test, different payloads (max 3.9 kg) are hung on it to reach a similar max F_R value as the human arm with targeted loads (0.5 and 1 kg). On the other hand, in the human tests, the effort-compensation device is worn by the participants (see Fig.1.7 for S_1), and the data including T_E, P_{Max}, and W_a are illustrated in Table.4.3. A simple calibration phase is designed to measure them.

In both tests, force references are generated using (2.3). For the benchtop test, l_a, l_l, and W_a are considered as 127 mm (lever length between O_3 and the point of W_a), $b + c$ (load lever length), and 0.42 kg, respectively. Moreover, for the human experiments, l_a, and l_l are taken into account as it is stated in section-2.1. Similar sensors (i.e., load cell, EMG, encoders), filters, and control gains as in section-4.1 are used in the experiments. Additionally, the velocity of the spool (ω) is also recorded.

4.2.1. Benchtop Experimental Protocol

Three experiments are conducted to validate the developed power-aware load releasing method. Experiment-A is designed without defining a power limit. First, the user varies arbitrarily the link position under 2 kg payload to represent the flexion/extension movement. Then, this load is removed suddenly from the link at a position to show the problem of sudden power increment on the cable. In experiment-B, the power threshold is defined as 1 Watt (W) based on a cyclic motion for 2 kg load with the desired velocity of the link, which is $10°/s$ (ω_{d1}). The user is asked to conduct flexion/extension movement on the link with this velocity by following the avatar that is created in MATLAB®. Finally, the load is taken out at around 35°. In experiment-C, the payload is increased to 3.9 kg, and the link position is changed with $25°/s$ (ω_{d2}) by the user using the same simulation (different velocity) mentioned above. Also, the power threshold is set as 3 W, and the user is asked to remove 2 kg load at around 90° to show the performance of the controller

at a different load-releasing position.

4.2.2. Benchtop Experimental Results

In Fig.4.5b, the results of experiment-A are presented. At $t = 4.5$ s, the load is removed, and ω reaches up to 80°/s showing an unsafe movement due to the generated force reference for the load. When it comes to experiment-B results in Fig.4.6a, at $t = 4.2$ s, the load is taken out, and, β becomes zero since P_{Exo} exceeds the power limit (illustrated in green area) according to the condition in (3.5). Hence, the portion of F_L is eliminated, and the device is fed only the link mass compensation (F_A).

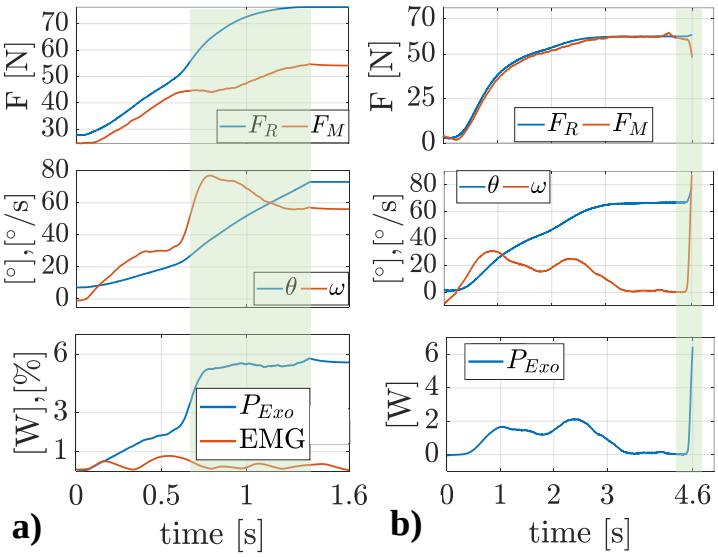

Figure 4.5: a) The experiment-1 results, where no power limit is defined in the exoskeleton, and 10 N load is released by S_1 to monitor force jump on the tendon. b) The experiment-A results where the link is hung 2 kg payload without setting P_{Max} in the benchtop setup.

In experiment-C results (see Fig.4.6b), since the load on the link is increased to 3.9 kg, the F_R reaches up to 60 N. Here, F_L is considered for 2 kg and 1.9 kg, separately, and only the former one is multiplied by β. Therefore, it can be clearly seen in Fig.4.6b (second row) that the dashed line and the orange line move together until $t = 5$s (pointed out in green area) in which the load-releasing starts. Then, when the power goes beyond the assigned limit, the force reference that belongs to 2 kg (F_{L1}) is multiplied by β, and its effect on F_R is terminated. Then, the user conducts free motion with the remaining load.

Important to note that, the adaptation time to new force reference in experiment-B and experiment-C are monitored as ≈ 0.4s, even though the load is released at 33° and 85° (see the zoomed views in Fig.4.6). During this interval, the link position increases 13°, and then settles to its previous position with minimal error, which is quite a rapid adaptation

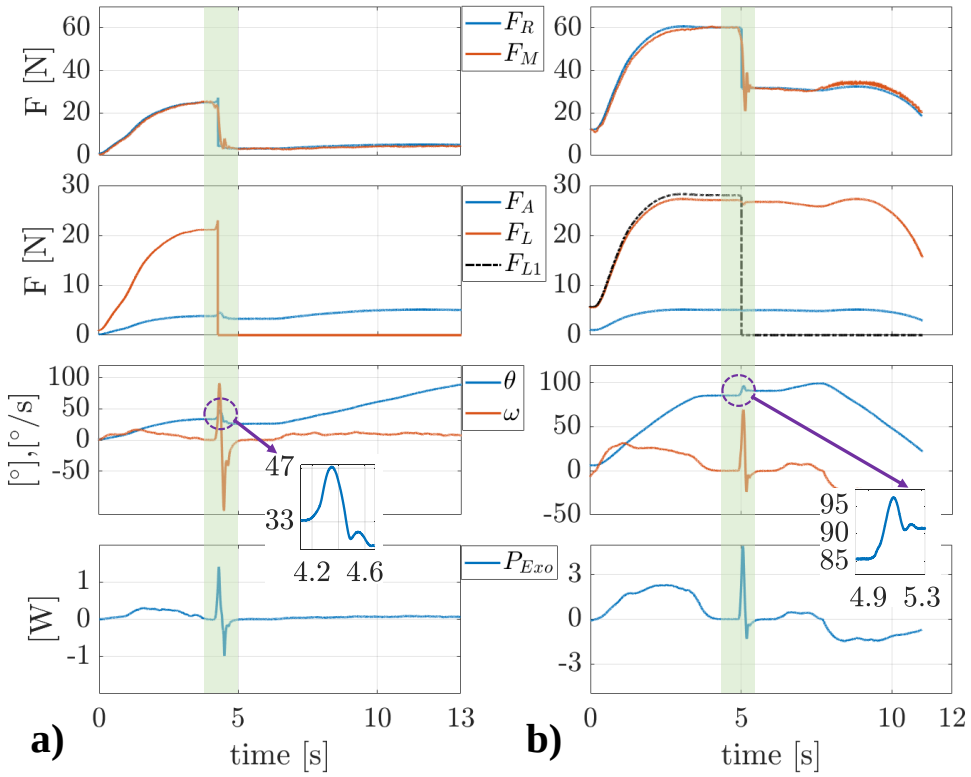

Figure 4.6: a) The experiment-B results where the load releasing is tested under 2 kg payload on benchtop setup with $P_{Max} = 1$ W, and b) The experiment-C results in which the load releasing is performed under 3.9 kg payload on the benchtop with $P_{Max} = 3$ W. Green area shows the time interval of load-releasing. The dashed purple circle illustrates the load-releasing phase for zoomed-view.

since both velocity and force of the tendon are taken into consideration to limit the power. Additionally, the root mean square (RMS) error of the tendon force ($F_R - F_M$) for experiment-B, and experiment-C are computed to be 0.84 N, and 1.91 N, respectively.

4.2.3. Human Experimental Protocol

The procedure is initiated with a calibration phase. First, the subjects' forearm weight is measured to estimate F_A, and to separate the effect of external load on the biceps muscle when the user holds a load. In other words, if a constant W_a is assigned for all subjects, and if this value is lower than the actual one, the users' effort may increase. Eventually, this could be sensed by EMG as a load at hand. Also, if the aforementioned weight is higher than another user's forearm weight, the device could apply excessive support to the user. Due to these reasons, the subjects are asked to let their arm be compensated by the exoskeleton at 90°. Making use of the measured tendon force and elbow position,

W_a values are computed through (2.3) for each participant.

After this step, the device is fed only F_A (see Fig.3.4) using the computed W_a, and the subjects follow the avatar (the similar simulation mentioned in 4.2.1) that performs the movement with ω_{d1}. Throughout this period, the normalized EMG values, which are acquired through maximum voluntary contraction (MVC [%]), are measured to compute the T_E (The details of the computation is mentioned in 3.2.1). Later on, participants are given W_{Max} as the load, and F_L is fed to device for this payload through (2.3). During this period, subjects pursue an avatar, which conducts flexion/extension movements with ω_{d2}, while measuring the power of the exoskeleton to record the P_{Max} value. At the end of this process, T_E, P_{Max}, and W_a parameters are determined for each subject.

The reason why P_{Max} values (see Table.4.3) differ for the subjects although there is a small difference in their forearm weight is because of the different elbow velocities. This happens due to the visual feedback (avatar) that subjects try to follow, and possible velocity errors have an effect on the power values. 0.5 W is also added to the measured power values as tolerance in case of sudden reflexive movements that might occur during the experiments.

To start with, experiment-1 is conducted to monitor the sudden force jump on the cable when W_{Max} is released from subject-1's (S_1) hand. No power limit is defined, and the user is assisted with this load and forearm weight. During the test, the EMG data of the subject is also recorded to make sure that there are no anticipatory movements. In experiment-2, only the load compensation algorithm is verified on S_1 for the same payload. The subject is asked to perform flexion movement following the avatar that conducts the desired motion with ω_{d1}. When the arm reaches the range of θ_C, the load is released to the subject-1's hand smoothly, and it is balanced instantaneously by S_1, which initiates the load compensation algorithm. Afterward, experiment-3 is carried out to validate only the load-releasing algorithm on the same subject for the same payload. To do that, the participant is informed to perform deliberate movement following an avatar that carries out the desired motion with ω_{d2}. Then, the load is released at a position without contracting the arm (i.e. naturally).

Next, experiment-4 is conducted to verify the developed load-compensation and load-releasing algorithms together in the same season through two different payloads (0.5 kg and 1 kg) on 8 subjects. The participants perform the same protocol mentioned in experiment-2 (load-compensation), and experiment-3 (load-releasing), consecutively. Finally, experiment-5 is carried out, and the subjects execute flexion/extension movements with ω_{d2} following the avatar. In this case, the exoskeleton is powered off, and the cable

is slacked. The goal is to observe the effort reduction on the biceps muscle thanks to the load-compensation and release algorithm. Throughout the human experiments, 10 minutes rest is given to the subjects in between 0.5 kg and 1 kg payload tests to minimize the development of fatigue.

4.2.4. Human Experimental Results

According to the experiment-1 result in Fig.4.5a, the subject starts doing flexion movement until $t = 0.8$ s, and then releases the object. It is clear that the device moves the arm $\approx 60°$ in 1 second (no anticipatory movements are observed on EMG data), and then the system is powered off immediately. As expected, P_{Exo} also sharply rises up to 6 W, and this behavior is not safe. Thus, P_{Max} is defined in experiment-3 (see Fig.4.7b), and the results show that when the load is released, the device adapts to only F_A eliminating the F_L in 0.4 s thanks to the β term in the power-aware control strategy.

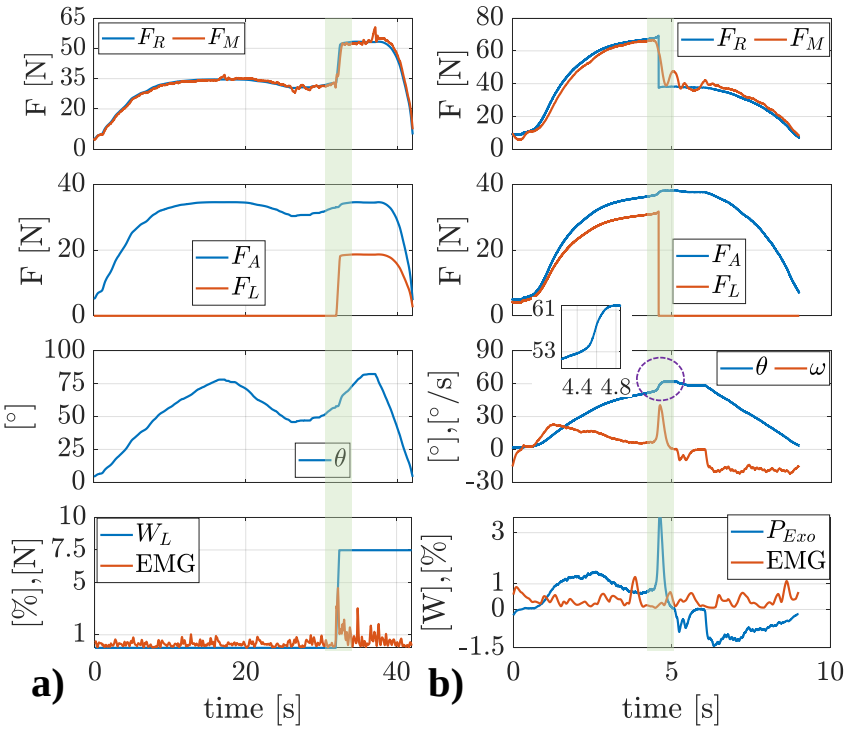

Figure 4.7: (a) The experiment-2 results of S_1 where only load-compensation algorithm is tested for 1 kg load, and then only load-release is performed for the same payload on S_1 with $P_{Max} = 3$ W in experiment-3 (b).

When the experiment-2 results are investigated in Fig.4.7a, the user performs deliberate movement until $t = 30$s. After that, the object is held by the user, and EMG goes above T_E. This triggers the load-compensation algorithm, and F_L starts to increase until EMG

reduces below the minimum effort level. After that, W_L is computed, and F_L is included in the force reference together with F_A (Fig.4.7a). The summation of these two terms is presented in the first row of the same figure (F_R).

Regarding the experiment-4 results in Fig.4.8, S_1 executes flexion movement until $t = 4$ s (a), and $t = 2$ s (b). During those periods, P_{Exo} does not exceed the P_{Max}, and F_L is zero since EMG is below T_E. Hence, only F_A is transferred to the wearer. When the load is released to the users' hand, the EMG increases (most bottom plots), and this initiates the load-estimation algorithm by generating F_L. As soon as EMG settles below T_E, the W_L is computed. Then, S_1 performs free-motions, and releases the load around $t = 30$ s, and $t = 35$ s for 0.5 kg, and 1 kg, respectively. At those instants, P_{Exo} surpasses the P_{Max}, and F_L becomes zero. Important to note that, although the objects are released at different positions (see Z.5 and Z.6) the adaptation time to only arm support during the load-releasing is around 0.6s.

The results of S_2, and S_3 for the same experiment are shown in Fig.4.9. In this case, the P_{Max}, and T_E are different from S_1 (see Table.4.3), which changes the EMG trends among subjects for the load-compensation phases. The fluctuations on F_M during the load-releasing phase comprises from the bungee elastic element integrated in the actuator design. To clarify, since F_L is eliminated from F_R as a step signal, the bungee acts as a mechanical filter between motor and the arm, transmitting this sudden change of motor to the user in a compliant way (shock absorbing). Additionally, the load-releasing and load-compensation time values are reported through zoomed views in Fig.4.8, and Fig.4.9. The load change duration is taken into account when F_M settles on F_R after the load-releasing or compensation phase. Throughout the load-releasing phases, the effort on EMG is monitored below T_E value, which demonstrates that the device naturally adapts the assistance to the remaining payload without disturbing the users' comfort.

Finally, the data of all subjects for experiment-4 are presented in Table.4.3, and statistical analysis is carried out in MATLAB®for the effort reductions, load compensation time (t_1), and load release time (t_2) with the level of significance 0.05. If p (p-value) is above this value, this means that the data is not significantly different. Otherwise, there is a significant difference among the selected data.

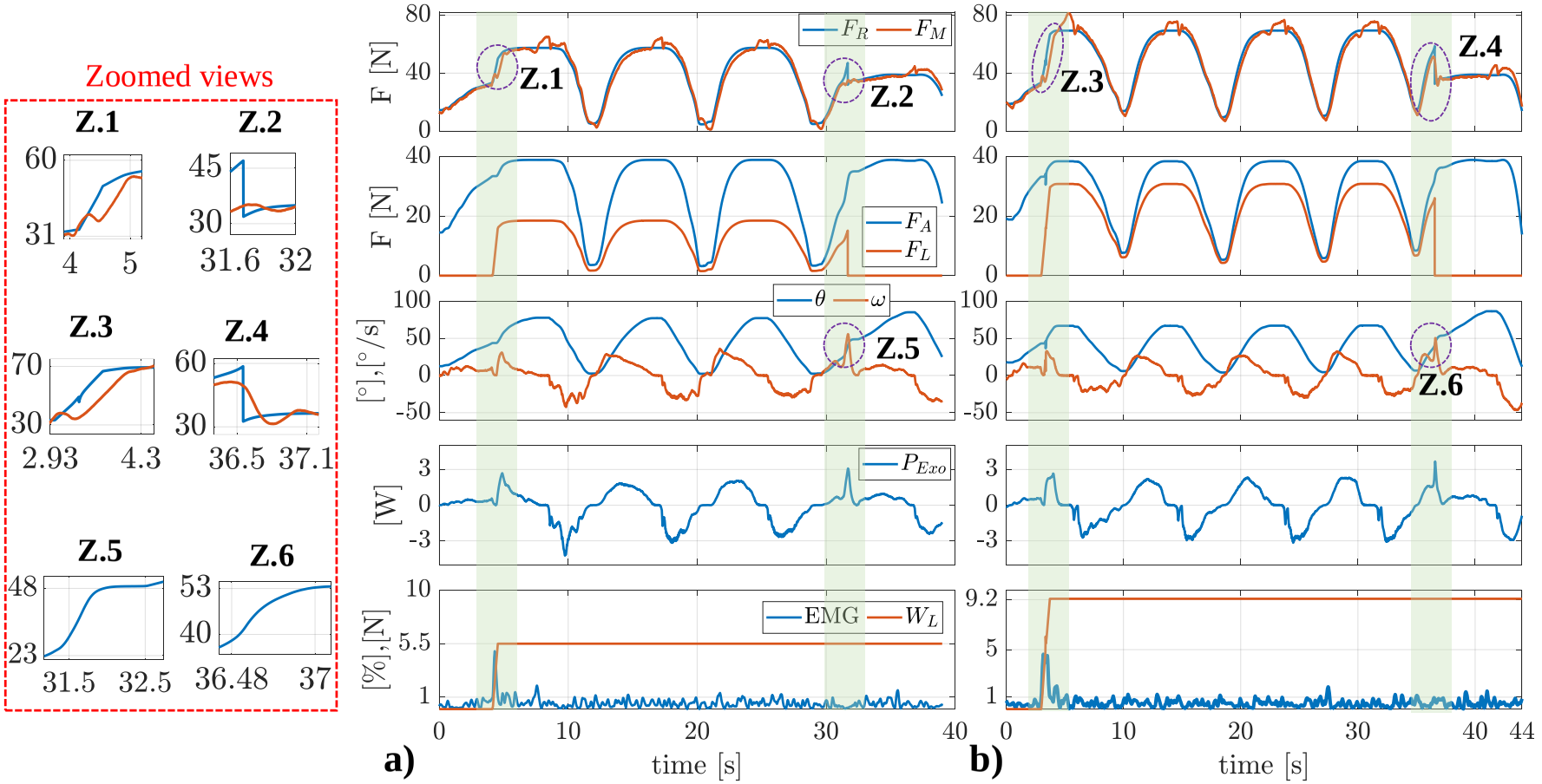

Figure 4.8: The results of experiment-4 where both load compensation and load release algorithms are tested for S_1 with 0.5 kg (a), and 1 kg (b). The green area shows the time interval of load-compensation and load-releasing. P_{Max} is defined for two payloads to be 3 W. Dashed purple circle points out the load transition phases.

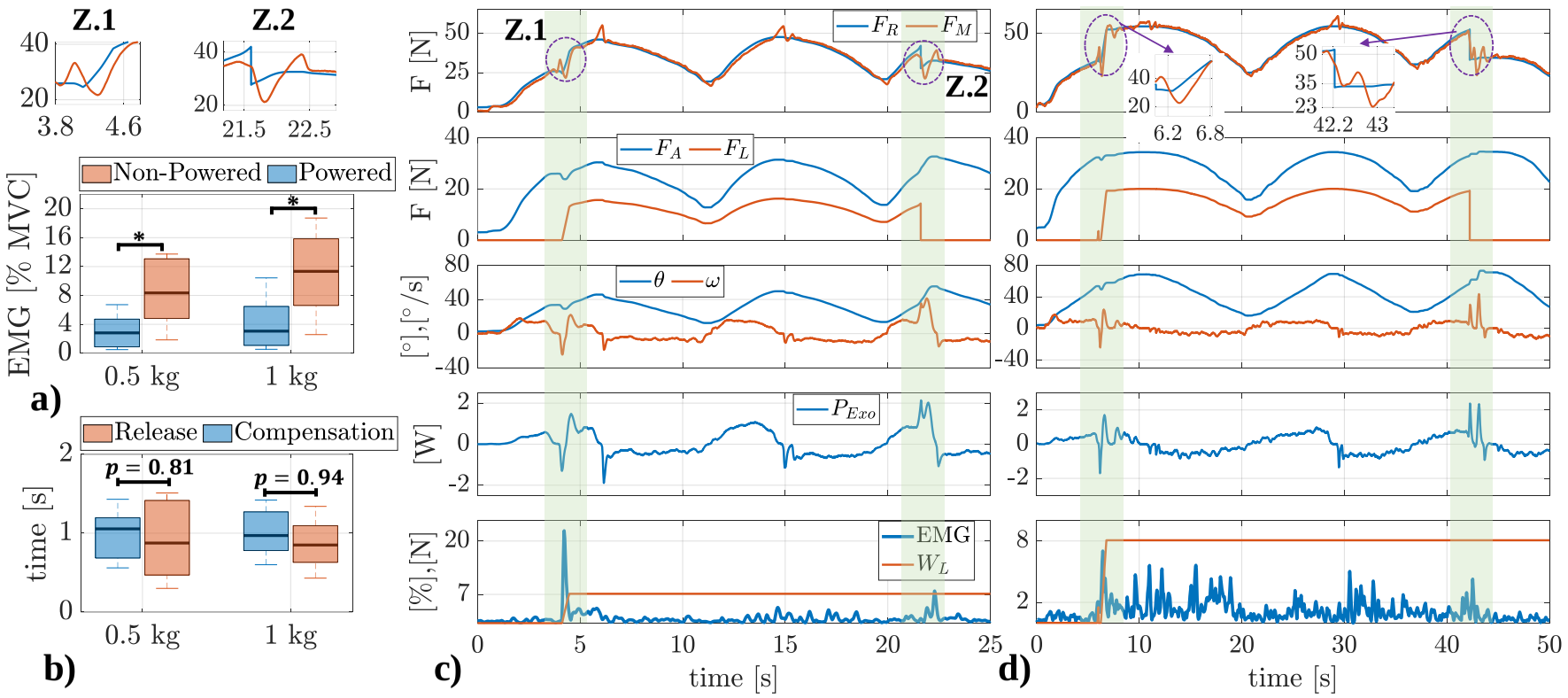

Figure 4.9: The results of experiment-4 in which both load compensation and load release are performed for S_2 (c), and S_3 (d) with 1 kg. The comparison of effort-reduction for with and without exoskeleton among 8 subjects for 0.5 and 1 kg (a), and the load-compensation and releasing time (b). The green area shows the load transition phases. $^*p < 0.05$.

For the effort reduction results, Wilcoxon rank sum test is carried out since the data is not normally distributed. p is acquired to be less than 0.05 for both payloads. This concludes that the data in between powered and non-powered cases are significantly different, which is an expected outcome. When it comes to t_1, and t_2, Wilcoxon signed rank test is conducted, and the desired median value of t_1, and t_2 is applied to be 1 second (targeted load-estimation time (t_t), in (3.2)). According to the results, p (time) values are acquired to be 0.81 (t_1), and 0.94 (t_2), for 0.5 kg and 1 kg, respectively. This demonstrates that the results are statistically not different, showing trivial differences around the desired median value. Furthermore, the mean value±standard deviation (payload) of the t_1 are calculated 0.98 ± 0.31 (0.5 kg), and 1 ± 0.29 (1 kg), and it is also computed for t_2 to be 0.91 ± 0.49 (0.5 kg), and 0.86 ± 0.3 (1 kg). The reason why the load-releasing time for 0.5 kg is slightly higher than 1 kg (see Fig.4.9) is because P_{Max} is assigned by considering 1 kg payload at the beginning instead of the online estimated loads. Thus, the worst-case scenario is taken into account in the test procedure. Lastly, the mean value±standard deviation (payload) of the W_L estimations are computed as 5.59 ± 0.52 N (5 N), and 8.74 ± 1.08 N (10 N) both of which are under the tolerance of the desired W_L values. Additionally, the mean value±standard deviation (payload) of the minimum/maximum elbow positions [°] are reported to be $11.97 \pm 5.31/74.2 \pm 7.76$ (0.5 kg), and $10.63 \pm 7.27/69.3 \pm 10.55$ (1 kg). The reason for the variations on θ_{Max} is that the participants are informed to conduct deliberate movement while following the avatar. This allows us to acquire similar arm velocities as that of the avatar, and eventually to keep the P_{Exo} below P_{Max} value unless there is load release action.

Table 4.3: Experiment-4 Results and the determined thresholds of the subjects

a, b, c, d : 50, 100, 50, 150 [mm]	**Subject-1**		**Subject-2**		**Subject-3**		**Subject-4**		**Subject-5**		**Subject-6**		**Subject-7**		**Subject-8**	
T_E [%], P_{Max} [W], W_a [N]	1, 3, 27		2, 2, 24		2, 2, 25		3, 1.5, 24		9, 3.2, 25		3.5, 3, 22		4, 2.5, 25		7, 2.5, 21	
Payload [kg]	**0.5**	**1**	**0.5**	**1**	**0.5**	**1**	**0.5**	**1**	**0.5**	**1**	**0.5**	**1**	**0.5**	**1**	**0.5**	**1**
W_L [N]	5.5	9.2	4.6	7.1	5.1	8.07	6.2	7.58	6.05	8.5	5.9	9.8	5.8	10.1	5.5	9.5
t_1 [s]	1	1.36	0.56	0.68	0.61	0.6	1.16	1.42	0.76	0.92	1.43	0.88	1.23	1.02	1.11	1.18
t_2 [s]	0.4	0.64	1.37	1.13	0.72	0.78	1.46	1.34	0.3	0.62	1.51	0.92	0.54	0.43	1.03	1.06
θ_{Max} [°]	77.3	70.9	63.5	50.1	71.2	69.4	66.6	65	82.2	84.7	77.4	64.9	69.4	68.3	85.8	80.8
θ_{Min} [°]	1.6	1.8	15.4	9.5	13.2	16.4	9.9	9.3	7.2	9.1	16.8	2.8	16.2	11.4	15	24.5
Force Error [N]	3.26	4.06	2.15	2.25	2.62	1.86	1.55	1.64	3.39	3.35	2.65	3.06	4.84	3.72	3.51	4.65
Effort Reduction [%]	87.03	89.4	45	54.4	87.1	88.4	73.2	68.4	51.05	63.1	62.5	75.2	71.01	44.2	54.4	53.04

T_E, P_{Max}, W_a, W_L, t_1, t_2 represent the minimum effort level, the maximum power, measured forearm weight, estimated load, load compensation time, and load release time, respectively. a, b, c, d are the dimensions of the arm attachments in mm and identified the same value for all the subjects. θ_{Max}, and θ_{Min} are the measured maximum and minimum elbow positions of the subjects.

5 | Discussions and Conclusions

5.1. Discussions

In this chapter, other relevant observations of the actuation system, design and adaptive control validation tests are discussed. Starting from the experiment-1 results of design validation test in chapter-4.1.1, the motion range is measured as 95° under 4 kg load (max $F_R \cong 65$N in Fig.4.1). However, for the human tests, the motion range of the S_1, whose F_R value is highest among the subjects, can perform up to $\cong 80°$. The reason for this dissimilarity arises from the compliant coupling design of human attachments. As expected, the force transmission for the link is more accurate than the human arm, which is compliant and leads to a force loss during the assistance due to small sliding on the arm attachments. Hence, the bungee elongation is more for the arm than the link under the same F_R. Therefore, the required ball-screw stroke to generate the max F_R increases, and the device size has to be enlarged to perform the same motion range as that of the benchtop setup. On the other hand, for the lower F_R values such as S_2, the motion range reaches up to 88°, which justifies the above hypothesis.

Additionally, the average force error of all subjects in human experiments of design validation test (see Table.4.2) is calculated as 4.88 N, which is partially due to the low resolution of the motor mentioned in Sec.3.1.1, and the response delay of the actuation system due to the fast movements. This results should be improved in the future. However, we believe that the effort reduction percentages are significant despite the current control errors.

As a limitation, the developed assistive device can be operated in such a way that the upper arm is always in a vertical state. This limited way of working should be refined in the future to enhance the applicability of the device to a variety of tasks.

On the other hand, investigating the other hybrid soft exoskeletons assistive torque (Nm) / device weight (kg) ratio (excluding the power supply), 3.4/2 in [65], 21/7.5 in [31], 10/ $\approx$ 2.5 in [38], and 5/2.45 in [57]. Moreover, we found in [66] that the efficiency of electric motor-tendon unit-based exosuits is 0.6.

Considering our device, it can generate up to 6.8 Nm torque with 1.6 kg weight (including arm attachments) with 0.54 power efficiency, which has a higher torque/weight ratio than the above-mentioned works. The reason for the small difference in efficiency between ours and other works may stem from the energy dissipation property of the elastic element. However, we believe that the advantages of having a high damping ratio are crucial to mimic the same characteristic of our muscles [40], absorbing the impulsive forces, and achieving a compliant force transmission to limbs.

When it comes to adaptive control validation test results, the average load-releasing time for the two payloads in human experimental results is acquired as 0.89 second (see Table.4.3). However, as expected, the load-releasing time on benchtop setup is sharply lower than human, measured as 0.4 s in Fig.4.6. The reason for this is due to the compliant coupling between the exoskeleton and humans as well as load estimation errors, which causes to demonstrate lower forces on the tendon, and eventually increases the time duration to reach the assigned power limit.

However, we believe that the implementation of power in the area of exoskeletons for load-transition in force control has significant advantages since we intuitively change the force reference without increasing the effort on humans or setting manually the payload as it has done already in the literature [23],[47]. Additionally, the method can be applied in any force/torque controlled assistive device including rehabilitation and, active daily life exoskeletons for different limbs such as shoulder, back, or even knee, as long as the torque and the velocity of the joint are measured (minimum requirement) for the computation of P_{Exo}.

5.2. Conclusions

In this thesis, the design and the control of a new assistive device to be used in manufacturing lines is presented. First, a design methodology was carried out starting from the torque and the motion range of the elbow. Then, an endless shape bungee was selected as the elastic element to achieve complaint force transmission between the human and the device. Next, a spool system was developed, and its force analysis was conducted to calculate the desired elastic force in the selection of the bungee, the motor, and the ball screw. Next, the mechanical design was optimized through the methodology, and then the FEA simulations were carried out for the critical parts to avoid stretching in the real prototype. Moreover actuator verification tests were conducted with and without bungee element to demonstrate its effectiveness at high frequency movements.

Results demonstrated that, the device isolated the vibrations 50.74% with respect to the

no-bungee case. Also, the damping ratio index of the mechanism is estimated, which is 56.14% more than that of no-bungee setup. Furthermore, an equivalent industrial painting task was designed to evaluate the device on 6 human subjects. A sensitivity analysis was performed to verify the adaptability of the device to different arm specifications. The mean value±standard deviation of the measured elbow velocities [$^\circ/s$] and maximum positions [$^\circ$] are 22.38 ± 5.03, and 78.8 ± 4.89, respectively. Moreover, the mean value±standard deviation of average effort reduction [%] values among subjects are computed as 64.42 ± 11.2. It is clear that the target values in Table.2.1 are acquired with a marginal error thanks to the developed design methodology in Section 2, which is unique to our design and provides us with realistic evidence through parametric calculations before manufacturing the prototype.

Apart from the contributions on design and its overall validation, adaptive control methods are developed to increase the flexibility, and usability of the effort-compensation device. A new control strategy is presented for sudden unloading tasks through the power of the force-controlled elbow effort-compensation device. First, the developed method is tested on a benchtop setup hanging 2 kg and 3.9 kg payloads, at different link speeds, and different load-releasing positions. Then, load estimation is also accomplished through a control strategy utilizing EMG sensor data attached to the user's biceps muscle. Later on, load-releasing and load-compensation operations are carried out separately on a subject. Finally, the overall scenario is verified for both actions consecutively in the same experiment on 8 participants with different payloads, different arm speeds, and different load-releasing arm positions. In addition, the subjects performed the desired tasks through the simulation without the exoskeleton to show the strength of the developed control method in terms of effort reduction. Results show that the mean value±standard deviation of the effort reduction [%] among subjects for 0.5 kg and 1 kg is 66.42 ± 15.92, and 67.11 ± 16.49, respectively.

As a future study, we aim to conduct the load compensation and release algorithm in different experimental conditions such as blindfolded to monitor the t_1, and t_2 values under unpredictable perturbations as in [17]. Also, we plan to test the algorithm in more repetitive use cases such as pick and place in a real industrial scenario.

6 | Related Publications and Patents

[A1] **E.Mobedi**, W. Kim, M. Leonori, N. G. Tsagarkis, A. Ajoudani, "Design and Control of an Assistive Device for Elbow Effort-Compensation." IEEE/ASME Transactions on Mechatronics, DOI: 10.1109/TMECH.2023.3267681.

[A2] **E.Mobedi**, S. Hjorth, W. Kim, E. De Momi, N. G. Tsagarkis, A. Ajoudani, "A Power-Aware Control Strategy for an Elbow Effort-Compensation Device." IEEE Robotics and Automation Letters, DOI:10.1109/LRA.2023.3282385.

[A3] **E.Mobedi**, W. Kim, E. De Momi, N. G. Tsagarkis, A. Ajoudani, "A Soft Assistive Device for Elbow Effort-Compensation." IEEE/RSJ International Conference on Intelligent Robots and Systems (IROS), 2021.

[A4] **E.Mobedi** and A. Ajoudani, "A Movement Assistive Device for the Elbow Joint", European Patent Application, EP4144331, 2023.

Bibliography

[1] T. Abe, S. Koizumi, H. Nabae, G. Endo, K. Suzumori, N. Sato, M. Adachi, and F. Takamizawa. Fabrication of "18 weave" muscles and their application to soft power support suit for upper limbs using thin mckibben muscle. *IEEE Robotics and Automation Letters*, 4(3):2532–2538, 2019. doi: 10.1109/LRA.2019.2907433.

[2] A. Ajoudani, N. Tsagarakis, and A. Bicchi. Tele-impedance: Teleoperation with impedance regulation using a body–machine interface. *The International Journal of Robotics Research*, 31(13):1642–1656, 2012.

[3] A. T. Asbeck, R. J. Dyer, A. F. Larusson, and C. J. Walsh. Biologically-inspired soft exosuit. In *2013 IEEE 13th International Conference on Rehabilitation Robotics (ICORR)*, pages 1–8. IEEE, 2013.

[4] T. M. Burton, R. Vaidyanathan, S. C. Burgess, A. J. Turton, and C. Melhuish. Sensitivity analysis of a parametric hand exoskeleton designed to match natural human grasping motion. In *Conference Towards Autonomous Robotic Systems*, pages 390–401. Springer, 2012.

[5] T. Bützer, O. Lambercy, J. Arata, and R. Gassert. Fully wearable actuated soft exoskeleton for grasping assistance in everyday activities. *Soft robotics*, 8(2):128–143, 2021.

[6] L. Cappello, A. Pirrera, P. Weaver, and L. Masia. A series elastic composite actuator for soft arm exosuits. In *2015 IEEE International Conference on Rehabilitation Robotics (ICORR)*, pages 61–66. IEEE, 2015.

[7] L. Cappello, D. K. Binh, S.-C. Yen, and L. Masia. Design and preliminary characterization of a soft wearable exoskeleton for upper limb. In *2016 6th IEEE International Conference on Biomedical Robotics and Biomechatronics (BioRob)*, pages 623–630, 2016. doi: 10.1109/BIOROB.2016.7523695.

[8] L. Cappello, D. K. Binh, S.-C. Yen, and L. Masia. Design and preliminary characterization of a soft wearable exoskeleton for upper limb. In *2016 6th IEEE in-*

ternational conference on biomedical robotics and biomechatronics (BioRob), pages 623–630. IEEE, 2016.

[9] L. Cappello, M. Xiloyannis, B. K. Dinh, A. Pirrera, F. Mattioni, and L. Masia. Multistable series elastic actuators: Design and control. *Robotics and Autonomous Systems*, 118:167–178, 2019.

[10] B. Celebi, M. Yalcin, and V. Patoglu. Assiston-knee: A self-aligning knee exoskeleton. In *2013 IEEE/RSJ International Conference on Intelligent Robots and Systems*, pages 996–1002. IEEE, 2013.

[11] M. Cenciarini and A. M. Dollar. Biomechanical considerations in the design of lower limb exoskeletons. In *2011 IEEE International conference on rehabilitation robotics*, pages 1–6. IEEE, 2011.

[12] D. Chiaradia, M. Xiloyannis, C. W. Antuvan, A. Frisoli, and L. Masia. Design and embedded control of a soft elbow exosuit. In *2018 IEEE International Conference on Soft Robotics (RoboSoft)*, pages 565–571. IEEE, 2018.

[13] D. Chiaradia, M. Xiloyannis, M. Solazzi, L. Masia, and A. Frisoli. Comparison of a soft exosuit and a rigid exoskeleton in an assistive task. In *Wearable Robotics: Challenges and Trends: Proceedings of the 4th International Symposium on Wearable Robotics, WeRob2018, October 16-20, 2018, Pisa, Italy 3*, pages 415–419. Springer, 2019.

[14] W. T. Dempster and G. R. Gaughran. Properties of body segments based on size and weight. *American journal of anatomy*, 120(1):33–54, 1967.

[15] B. K. Dinh, M. Xiloyannis, C. W. Antuvan, L. Cappello, and L. Masia. Hierarchical cascade controller for assistance modulation in a soft wearable arm exoskeleton. *IEEE robotics and automation letters*, 2(3):1786–1793, 2017.

[16] A. Ebrahimi. Stuttgart exo-jacket: An exoskeleton for industrial upper body applications. In *2017 10th International Conference on Human System Interactions (HSI)*, pages 258–263. IEEE, 2017.

[17] A. Forghani, R. Preuss, and T. Milner. Postural response characterization of standing humans to multi-directional, predictable and unpredictable perturbations to the arm. *Journal of Electromyography and Kinesiology*, 32:83–92, 2017.

[18] C. H. Glock, E. H. Grosse, W. P. Neumann, and A. Feldman. Assistive devices for manual materials handling in warehouses: a systematic literature review. *International Journal of Production Research*, 59(11):3446–3469, 2021.

[19] C. Gosselin, T. Laliberte, B. Mayer-St-Onge, S. Foucault, A. Lecours, V. Duchaine, N. Paradis, D. Gao, and R. Menassa. A friendly beast of burden: A human-assistive robot for handling large payloads. *IEEE Robotics & Automation Magazine*, 20(4): 139–147, 2013. doi: 10.1109/MRA.2013.2283651.

[20] D. Govin, L. Saenz, G. Athanasaki, L. Snyder, and P. Polygerinos. Design and development of a soft robotic back orthosis. In *Frontiers in Biomedical Devices*, volume 40789, page V001T10A001. American Society of Mechanical Engineers, 2018.

[21] M. Hagberg. Work load and fatigue in repetitive arm elevations. *Ergonomics*, 24(7): 543–555, 1981.

[22] M. Hagberg and D. Wegman. Prevalence rates and odds ratios of shoulder-neck diseases in different occupational groups. *Occupational and environmental medicine*, 44(9):602–610, 1987.

[23] M. Hosseini, R. Meattini, A. San-Millan, G. Palli, C. Melchiorri, and J. Paik. A semg-driven soft exosuit based on twisted string actuators for elbow assistive applications. *IEEE Robotics and Automation Letters*, 5(3):4094–4101, 2020.

[24] K. Huysamen, T. Bosch, M. de Looze, K. S. Stadler, E. Graf, and L. W. O'Sullivan. Evaluation of a passive exoskeleton for static upper limb activities. *Applied ergonomics*, 70:148–155, 2018.

[25] M. R. U. Islam and S. Bai. Payload estimation using forcemyography sensors for control of upper-body exoskeleton in load carrying assistance. *Modeling, Identification and Control*, 40(4):189–198, 2019. doi: 10.4173/mic.2019.4.1.

[26] L. Kapandji. The physiology of the joints-annoted diagrams of the mechanics of the human joints. *Upper limb*, pages 108–129, 1982.

[27] J. Kim, G. Lee, R. Heimgartner, D. Arumukhom Revi, N. Karavas, D. Nathanson, I. Galiana, A. Eckert-Erdheim, P. Murphy, D. Perry, et al. Reducing the metabolic rate of walking and running with a versatile, portable exosuit. *Science*, 365(6454): 668–672, 2019.

[28] W. Kim, S. Lee, M. Kang, J. Han, and C. Han. Energy-efficient gait pattern generation of the powered robotic exoskeleton using dme. In *2010 IEEE/RSJ International Conference on Intelligent Robots and Systems*, pages 2475–2480. IEEE, 2010.

[29] W. Kim, H. Lee, D. Kim, J. Han, and C. Han. Mechanical design of the hanyang exoskeleton assistive robot(hexar). In *2014 14th International Conference on Control,*

Automation and Systems (ICCAS 2014), pages 479–484, 2014. doi: 10.1109/ICCAS.2014.6988049.

[30] Y. G. Kim, M. Xiloyannis, D. Accoto, and L. Masia. Development of a soft exosuit for industrial applications. In *2018 7th IEEE International Conference on Biomedical Robotics and Biomechatronics (Biorob)*, pages 324–329, 2018. doi: 10.1109/BIOROB.2018.8487907.

[31] Y. G. Kim, K. Little, B. Noronha, M. Xiloyannis, L. Masia, and D. Accoto. A voice activated bi-articular exosuit for upper limb assistance during lifting tasks. *Robotics and Computer-Integrated Manufacturing*, 66:101995, 2020.

[32] M. Laffranchi, N. G. Tsagarakis, and D. G. Caldwell. Analysis and development of a semiactive damper for compliant actuation systems. *IEEE/ASME Transactions on Mechatronics*, 18(2):744–753, 2013. doi: 10.1109/TMECH.2012.2184293.

[33] E. P. Lamers, A. J. Yang, and K. E. Zelik. Feasibility of a biomechanically-assistive garment to reduce low back loading during leaning and lifting. *IEEE Transactions on Biomedical Engineering*, 65(8):1674–1680, 2017.

[34] Y. Lee, J. Lee, B. Choi, M. Lee, S. Roh, K. Kim, K. Seo, Y. Kim, and Y. Shim. Flexible gait enhancing mechatronics system for lower limb assistance (gems l-type). *IEEE/ASME Transactions on Mechatronics*, 24(4):1520–1531, 2019.

[35] T. Lenzi, S. M. M. De Rossi, N. Vitiello, and M. C. Carrozza. Intention-based emg control for powered exoskeletons. *IEEE Transactions on Biomedical Engineering*, 59 (8):2180–2190, 2012. doi: 10.1109/TBME.2012.2198821.

[36] S. Lessard, P. Pansodtee, A. Robbins, J. M. Trombadore, S. Kurniawan, and M. Teodorescu. A soft exosuit for flexible upper-extremity rehabilitation. *IEEE Transactions on Neural Systems and Rehabilitation Engineering*, 26(8):1604–1617, 2018.

[37] N. Lotti, M. Xiloyannis, G. Durandau, E. Galofaro, V. Sanguineti, L. Masia, and M. Sartori. Adaptive model-based myoelectric control for a soft wearable arm exosuit: A new generation of wearable robot control. *IEEE Robotics & Automation Magazine*, 27(1):43–53, 2020.

[38] N. Lotti, M. Xiloyannis, F. Missiroli, C. Bokranz, D. Chiaradia, A. Frisoli, R. Riener, and L. Masia. Myoelectric or force control? a comparative study on a soft arm exosuit. *IEEE Transactions on Robotics*, 38(3):1363–1379, 2022. doi: 10.1109/TRO.2021.3137748.

[39] P. Maurice, J. Čamernik, D. Gorjan, B. Schirrmeister, J. Bornmann, L. Tagliapietra, C. Latella, D. Pucci, L. Fritzsche, S. Ivaldi, et al. Evaluation of paexo, a novel passive exoskeleton for overhead work. *Computer Methods in Biomechanics and Biomedical Engineering*, 22(sup1):S448–S450, 2019.

[40] T. E. Milner and C. Cloutier. Damping of the wrist joint during voluntary movement. *Experimental brain research*, 122(3):309–317, 1998.

[41] F. Missiroli, N. Lotti, E. Tricomi, C. Bokranz, R. Alicea, M. Xiloyannis, J. Krzywinski, S. Crea, N. Vitiello, and L. Masia. Rigid, soft, passive, and active: A hybrid occupational exoskeleton for bimanual multijoint assistance. *IEEE Robotics and Automation Letters*, 7(2):2557–2564, 2022.

[42] E. Mobedi, W. Kim, E. D. Momi, N. G. Tsagarakis, and A. Ajoudani. A soft assistive device for elbow effort-compensation. In *2021 IEEE/RSJ International Conference on Intelligent Robots and Systems (IROS)*, pages 9540–9547, 2021. doi: 10.1109/IROS51168.2021.9636771.

[43] M. Napolitano. 2012 warehouse/dc operations survey: mixed signals. *Logistics management (Highlands Ranch, Colo.: 2002)*, 51(11), 2012.

[44] C. O'Neill, T. Proietti, K. Nuckols, M. E. Clarke, C. J. Hohimer, A. Cloutier, D. J. Lin, and C. J. Walsh. Inflatable soft wearable robot for reducing therapist fatigue during upper extremity rehabilitation in severe stroke. *IEEE Robotics and Automation Letters*, 5(3):3899–3906, 2020. doi: 10.1109/LRA.2020.2982861.

[45] C. O'Neill, T. Proietti, K. Nuckols, M. E. Clarke, C. J. Hohimer, A. Cloutier, D. J. Lin, and C. J. Walsh. Inflatable soft wearable robot for reducing therapist fatigue during upper extremity rehabilitation in severe stroke. *IEEE Robotics and Automation Letters*, 5(3):3899–3906, 2020.

[46] D. Park and K.-J. Cho. Development and evaluation of a soft wearable weight support device for reducing muscle fatigue on shoulder. *PloS one*, 12(3):e0173730, 2017.

[47] D. Park, C. Di Natali, D. G. Caldwell, and J. Ortiz. Control strategy for shoulder-sidewinder with kinematics, load estimation, and friction compensation: Preliminary validation. *IEEE Robotics and Automation Letters*, 7(2):1278–1283, 2021.

[48] D. Park, S. Toxiri, G. Chini, C. D. Natali, D. G. Caldwell, and J. Ortiz. Shoulder-sidewinder (shoulder-side wearable industrial ergonomic robot): Design and evaluation of shoulder wearable robot with mechanisms to compensate for joint misalign-

ment. *IEEE Transactions on Robotics*, 38(3):1460–1471, 2022. doi: 10.1109/TRO.2021.3125854.

[49] S. J. Park and C. H. Park. Suit-type wearable robot powered by shape-memory-alloy-based fabric muscle. *Scientific reports*, 9(1):1–8, 2019.

[50] J. C. Perry, J. Rosen, and S. Burns. Upper-limb powered exoskeleton design. *IEEE/ASME transactions on mechatronics*, 12(4):408–417, 2007.

[51] D. Ranney, R. Wells, and A. Moore. Upper limb musculoskeletal disorders in highly repetitive industries: precise anatomical physical findings. *Ergonomics*, 38(7):1408–1423, 1995.

[52] M. Schalk, I. Schalk, T. Bauernhansl, J. Siegert, A. Esin, and U. Schneider. Influence of exoskeleton use on welding quality during a simulated welding task. *Wearable Technologies*, 3:e17, 2022.

[53] A. Schiele and F. C. Van Der Helm. Kinematic design to improve ergonomics in human machine interaction. *IEEE Transactions on neural systems and rehabilitation engineering*, 14(4):456–469, 2006.

[54] A. H. Stienen, E. E. Hekman, F. C. Van Der Helm, and H. Van Der Kooij. Self-aligning exoskeleton axes through decoupling of joint rotations and translations. *IEEE Transactions on Robotics*, 25(3):628–633, 2009.

[55] C. Thakur, K. Ogawa, T. Tsuji, and Y. Kurita. Soft wearable augmented walking suit with pneumatic gel muscles and stance phase detection system to assist gait. *IEEE Robotics and Automation Letters*, 3(4):4257–4264, 2018.

[56] C. M. Thalman, Q. P. Lam, P. H. Nguyen, S. Sridar, and P. Polygerinos. A novel soft elbow exosuit to supplement bicep lifting capacity. In *2018 IEEE/RSJ International Conference on Intelligent Robots and Systems (IROS)*, pages 6965–6971, 2018. doi: 10.1109/IROS.2018.8594403.

[57] L. Tiseni, M. Xiloyannis, D. Chiaradia, N. Lotti, M. Solazzi, H. Van der Kooij, A. Frisoli, and L. Masia. On the edge between soft and rigid: an assistive shoulder exoskeleton with hyper-redundant kinematics. In *2019 IEEE 16th International Conference on Rehabilitation Robotics (ICORR)*, pages 618–624. IEEE, 2019.

[58] N. G. Tsagarakis, S. Morfey, H. Dallali, G. A. Medrano-Cerda, and D. G. Caldwell. An asymmetric compliant antagonistic joint design for high performance mobility. In *2013 IEEE/RSJ International Conference on Intelligent Robots and Systems*, pages 5512–5517. IEEE, 2013.

[59] W. van Dijk, H. van der Kooij, and E. Hekman. A passive exoskeleton with artificial tendons: Design and experimental evaluation. In *2011 IEEE International Conference on Rehabilitation Robotics*, pages 1–6, 2011. doi: 10.1109/ICORR.2011.5975470.

[60] B. Vanderborght. *Unlocking the potential of industrial human–robot collaboration: A vision on industrial collaborative robots for economy and society.* Publications Office of the European Union, 2 2020. ISBN 978-92-76-11248-8.

[61] N. Villa, E. Mobedi, and A. Ajoudani. A contact-adaptive control framework for co-manipulation tasks with application to collaborative screwing. In *2022 31st IEEE International Conference on Robot and Human Interactive Communication (RO-MAN)*, pages 1131–1137, 2022. doi: 10.1109/RO-MAN53752.2022.9900522.

[62] N. Vitiello, T. Lenzi, S. Roccella, S. M. M. De Rossi, E. Cattin, F. Giovacchini, F. Vecchi, and M. C. Carrozza. Neuroexos: A powered elbow exoskeleton for physical rehabilitation. *IEEE Transactions on Robotics*, 29(1):220–235, 2013.

[63] A. Voilqué, J. Masood, J. Fauroux, L. Sabourin, and O. Guezet. Industrial exoskeleton technology: Classification, structural analysis, and structural complexity indicator. In *2019 Wearable Robotics Association Conference (WearRAcon)*, pages 13–20, 2019. doi: 10.1109/WEARRACON.2019.8719395.

[64] M. Wehner, B. Quinlivan, P. M. Aubin, E. Martinez-Villalpando, M. Baumann, L. Stirling, K. Holt, R. Wood, and C. Walsh. A lightweight soft exosuit for gait assistance. In *2013 IEEE international conference on robotics and automation*, pages 3362–3369. IEEE, 2013.

[65] M. Xiloyannis, E. Annese, M. Canesi, A. Kodiyan, A. Bicchi, S. Micera, A. Ajoudani, and L. Masia. Design and validation of a modular one-to-many actuator for a soft wearable exosuit. *Frontiers in Neurorobotics*, 13:39, 2019.

[66] M. Xiloyannis, R. Alicea, A.-M. Georgarakis, F. L. Haufe, P. Wolf, L. Masia, and R. Riener. Soft robotic suits: State of the art, core technologies, and open challenges. *IEEE Transactions on Robotics*, 2021.

[67] W. Yu, J. Rosen, and X. Li. Pid admittance control for an upper limb exoskeleton. In *Proceedings of the 2011 American Control Conference*, pages 1124–1129, 2011. doi: 10.1109/ACC.2011.5991147.

[68] T. Zhang, M. Tran, and H. Huang. Design and experimental verification of hip exoskeleton with balance capacities for walking assistance. *IEEE/ASME Transactions on mechatronics*, 23(1):274–285, 2018.

[69] Y. Zhang, A. Ajoudani, and N. G. Tsagarakis. Exo-muscle: A semi-rigid assistive device for the knee. *IEEE Robotics and Automation Letters*, 6(4):8514–8521, 2021. doi: 10.1109/LRA.2021.3100609.

[70] Y. M. Zhou, C. Hohimer, T. Proietti, C. T. O'Neill, and C. J. Walsh. Kinematics-based control of an inflatable soft wearable robot for assisting the shoulder of industrial workers. *IEEE Robotics and Automation Letters*, 6(2):2155–2162, 2021. doi: 10.1109/LRA.2021.3061365.

[71] A. Zoss, H. Kazerooni, and A. Chu. Biomechanical design of the berkeley lower extremity exoskeleton (bleex). *IEEE/ASME Transactions on Mechatronics*, 11(2): 128–138, 2006. doi: 10.1109/TMECH.2006.871087.

List of Figures

List of Tables

Acknowledgements

I would first like to thank my thesis advisor, Dr. Arash Ajoudani for his continuous support, always availability, humanitarian approach, motivation, and giving me a part of work from a prestigious European project SOPHIA.

Despite the difficulties that I faced with in the beginning of my PhD such as starting my study remotely due to COVID issues, he was always giving feedback, and connecting me with several expert roboticist including Dr. Nikos Tsagarakis, and Assistant Prof. Wansoo Kim. Therefore, I would also like to express my sincere gratitude to Dr. Tsagarakis and his Lab, Humanoid and Human Centred Mechatronics, for their support to my work.

Also, I would like to thank my all colleagues in Human Robot Interfaces and Interaction Lab for their hospitality, friendship, and technical support.

I also would like to thank to Marco Simonini who helped me so much to solve the permesso di soggiorno issues during the COVID period, and allowing me to come to Italy. Without his dedication, it would be very hard for me to solve those bureaucratic problems. I also acknowledge to Prof Elena De Momi for her feedback on my work. In addition, I thank to my thesis reviewers Prof Lorenzo Masia and Prof Herman van der Kooij for their valuable feedbacks and comments to improve the quality of my thesis.

Finally, I must express my very profound gratitude to my parents, Ilkay and Muhammed Mobedi, and my uncle Prof Moghtada Mobedi, for providing me with unfailing support and continuous encouragement during my years in Italy. This achievement would not have been possible without them. Thank you..